MESENCHYMAL PHENOTYPE OF CHOLANGIOCYTES PLAYS AN INTEGRAL ROLE IN THE REGULATION OF BILIARY SENESCENCE AND LIVER FIBROSIS IN CHOLESTATIC LIVER DISEASES

A Dissertation

by

TIANHAO ZHOU

Submitted to the Office of Graduate and Professional Studies of
Texas A&M University
in partial fulfillment of the requirements for the degree of

DOCTOR OF PHILOSOPHY

Chair of Committee,	Shannon Glaser
Co-Chair of Committee,	Gianfranco Alpini
Committee Members,	Cynthia J. Meininger
	Chaodong Wu
Head of Department,	Carol Vargas

May 2020

Major Subject: Medical Sciences

ABSTRACT

Cholangiocytes are the epithelial cells lining the bile ducts in the liver and the target of cholestatic liver diseases, such as primary sclerosing cholangitis (PSC) and primary biliary cholangitis (PBC). Cholangiopathies are characterized by hepatic inflammation, ductular reaction, liver fibrosis and, eventually, carcinogenesis. Epithelial-mesenchymal transition (EMT) is an event by which epithelial cells lose their native characteristics and display functional properties of mesenchymal cells. Vimentin is a type III intermediate filament, and induction of vimentin in epithelial cells results in several important features of EMT, including the adoption of a mesenchymal shape, loss of desmosomes and increased focal adhesion and cell motility. Secretin receptor (SR) is only expressed by cholangiocytes, which plays a key role in the regulation of biliary damage and liver fibrosis.

The overall goal of this study was to evaluate whether EMT occurs in cholangiocytes and contributes to the progression of biliary senescence and liver fibrosis in cholestatic liver diseases. Male 12-week-old $Mdr2^{-/-}$ mice with or without vimentin Vivo-Morpholino treatment, $SR^{-/-}$ mice, $SR^{-/-}/Mdr2^{-/-}$ mice and their corresponding control groups were used for the *in vivo* studies. Staining was performed in liver sections for evaluation of (i) histological features using hematoxylin and eosin (H&E) staining; (ii) EMT by vimentin and E-cadherin; (iii) ductular reaction by CK-19; (iv) liver fibrosis by Sirius Red staining and Col1a1, and (v) biliary senescence by SA-β-gal and p16. TGF-β1 levels were measured in serum and cholangiocyte supernatants using ELISA kits. Liver

specimens from human PSC patients, human intrahepatic biliary epithelial cells (HIBEpiCs), and human hepatic stellate cell lines (HHSteCs) were also used to evaluate changes in EMT.

There was increased expression of a mesenchymal phenotype of cholangiocytes in $Mdr2^{-/-}$ mice, which was reduced by treatment with vimentin Vivo-Morpholino and genetic depletion of SR. Concomitant with reduced vimentin expression, there was decreased liver damage, ductular reaction, biliary senescence, liver fibrosis, and TGF-β1 secretion in $Mdr2^{-/-}$ mice treated with vimentin Vivo-Morpholino and $SR^{-/-}/Mdr2^{-/-}$ mice. Human PSC patients and derived cell lines had increased expression of vimentin and other mesenchymal markers compared to healthy controls and HIBEpiCs, respectively. *In vitro* silencing of vimentin in HIBEpiCs suppressed TGF-β1-induced EMT and fibrotic reaction. HHSteCs had decreased fibrotic response and increased cellular senescence after stimulation with cholangiocyte supernatant with reduced vimentin levels.

Our study demonstrated that loss of vimentin or SR reduces the mesenchymal phenotype of cholangiocytes, which leads to decreased biliary senescence and liver fibrosis. Inhibition of vimentin or SR may be a key therapeutic target in the treatment of cholangiopathies including PSC.

DEDICATION

This dissertation is dedicated to my family and many friends, thank you for encouraging me in all of my pursuits and inspiring me to follow my dreams. I am especially grateful to my parents, who supported me emotionally and financially; my wife, who stands by me through this entire journey. I always knew that you believed in me and wanted the best for me.

ACKNOWLEDGEMENTS

I would like to thank my committee chair, Dr. Glaser, and my committee members, Dr. Alpini, Dr. Meininger and Dr. Wu, for their guidance and support throughout the course of this research.

Thanks also go to my friends and lab colleagues and the department faculty and staff for making my time at Texas A&M University a great experience.

CONTRIBUTORS AND FUNDING SOURCES

Contributors

This work was supervised by a dissertation committee consisting of Dr. Shannon Glaser (advisor) and Gianfranco Alpini (co-advisor), Dr. Cynthia Meininger of the Department of Medical Physiology and Dr. Chaodong Wu of the Department of Nutrition and Food Science.

A portion of this dissertation research was conducted by Tianhao Zhou and the co-authors and was previously published in EBioMedicine [Oct 2019, 48, 130-142] and Laboratory Investigation [Nov 2018, 98 (11), 1449-1464].

All other work conducted for the dissertation was completed by the student independently.

Funding Sources

This work was made possible in part by the Hickam Endowed Chair, Gastroenterology, Department of Medicine, Indiana University; the VA Merit awards to Gianfranco Alpini (5I01BX000574) from the United States Department of Veteran's Affairs; Biomedical Laboratory Research and Development Service and NIH grants DK108959 (Heather Francis); AA026385 (Zhihong Yang); DK054811, DK076898, DK107310, DK110035, DK062975, AA025997 and AA025157 to Gianfranco Alpini, Shannon Glaser and Fanyin Meng; DK107682, AA025208, AA026917, AA026903 and CX000361 (to Suthat Liangpunsakul); and a grant award from PSC Partners Seeking a

Cure to Gianfranco Alpini. Its contents are solely the responsibility of the authors and do not necessarily represent the official views of the Department of Veterans Affairs.

NOMENCLATURE

abcb4	ATP binding cassette subfamily B member 4
ALP	alkaline phosphatase
α-SMA	alpha smooth muscle actin
BDL	bile duct ligation
BMDMs	bone marrow-derived macrophages
cAMP	cyclic adenosine monophosphate
CD11b	cluster of differentiation molecule 11B
CFTR	cystic fibrosis transmembrane conductance regulator
CCL2	C-C motif chemokine ligand 2
CCl_4	carbon tetrachloride
CK-19	cytokeratin-19
Col1a1	collagen, type I, alpha 1
DAPI	4’,6-diamidino-2-phenylindole
DAMPs	danger-associated-molecular-pattern molecules
ECM	extracellular matrix
ELISA	enzyme-linked immunosorbent assay
EMT	epithelial to mesenchymal transition
EpCAM	epithelial cell adhesion molecule
FFPE	formalin fixed paraffin embedded
Fn1	fibronectin 1

GAPDH	glyceraldehyde-3-phosphate dehydrogenase
H&E	hematoxylin & eosin
HSCs	hepatic stellate cells
HHSteCs	human hepatic stellate cell lines
HIBEpiCs	human intrahepatic biliary epithelial cells
HNF4α	hepatocyte nuclear factor 4 alpha
hPSCL	human PSC patient-derived cholangiocytes
IBDM	intrahepatic Bile Duct Mass
IL-1β	interleukin 1β
IL-6	interleukin 6
IL-33	interleukin 33
IPA	ingenuity pathway analysis
LCM	laser capture microdissection
LY-6C	lymphocyte antigen 6 complex, locus C
Mdr2	multidrug resistance gene 2
MDR3	multidrug resistance protein 3
MMP	matrix metallopeptidase
p16	cyclin dependent kinase inhibitor 2A
p21	cyclin-dependent kinase inhibitor 1
PBC	primary biliary cholangitis
PSC	primary sclerosing cholangitis
PCNA	proliferating cellular nuclear antigen

PCR	polymerase chain reaction
S100a4	S100 calcium binding protein A4
SA-β-gal	senescence associated β galactosidase
Sct	secretin
Smad	Sma genes and the Drosophila Mothers against decapentaplegic
SR	secretin receptor
SGOT	serum glutamic oxaloacetic
SGPT	alanine aminotransferase
TGF-β1	transforming growth factor-β1
TNF-α	tumor necrosis factor alpha
UDCA	ursodeoxycholic acid
VEGFA	vascular endothelial growth factor A
WT	wild type

TABLE OF CONTENTS

Page

LIST OF FIGURES

Page

LIST OF TABLES

Page

CHAPTER I

INTRODUCTION AND LITERATURE REVIEW

Cholangiopathies

Cholangiopathies, such as primary sclerosing holancgitis (PSC) and primary biliary cholangitis (PBC), are cholestatic liver diseases (targeting intra- and extra-hepatic cholangiocytes) that are characterized by hepatic inflammation, ductular reaction, liver fibrosis, cirrhosis and eventually liver cancer.

Cholangiocytes

Cholangiocytes are the epithelial cells lining the bile ducts in the liver. Although cholangiocytes comprise only ~5% of the cells in the liver, they are critical for modifying the composition of canalicular bile by secreting water, bicarbonate, and chloride ions (1, 2). Similar to other epithelial cells, cholangiocytes are polarized with distinct apical and basolateral plasma membranes. Heterogeneity in cholangiocyte morphology and function has been widely studied and manifests as different diameter and protein expression between small and large cholangiocytes (3, 4). Secretin receptor (SR), cystic fibrosis transmembrane conductance regulator (CFTR), and the chloride bicarbonate anion exchanger 2 (Cl^-/HCO_3^-) are expressed by large cholangiocytes but not small cholangiocytes. While large cholangiocyte proliferation is cyclic adenosine 3',5'-monophosphate- (cAMP-) dependent, proliferation of small cholangiocytes is dependent on intracellular Ca^{2+} release induced by inositol 1,4,5-trisphosphate (4-6). Under healthy conditions, cholangiocytes play an important physiological role to modify bile within the

bile duct lumen by a series of hormone-regulated cAMP-or Ca^{2+}-dependent activities, which are modulated by biliary constituents (including bile acids), extracellular signals (such as peptides, nucleotides, hormones and neurotransmitters) and physical forces (flow and pressure) through various intracellular signaling pathways (4, 5, 7). During liver injury, cholangiocytes can acquire a proliferative phenotype and secrete pro-inflammatory and pro-fibrotic chemokines, cytokines, as well as angiogenic growth factors, which leads to paracrine immune responses and the activation of hepatic stellate cells (HSCs, the major source of myofibroblasts in the liver) (8, 9). In addition, a subpopulation of cholangiocytes can undergo senescence and exhibit features of the senescence-associated secretory phenotype (SASP), a cell fate also characterized by the release of cytokines and chemokines (e.g., TGF-β1, p16, CCL2 and SA-β-gal) (10, 11).

Primary Sclerosing Cholangitis

PSC is a major type of chronic cholestatic liver disease, in which the bile ducts inside and outside the liver become inflamed and scarred. When the bile ducts are eventually narrowed or blocked, bile builds up in the liver and causes liver damage. Approximately 60%-70% of patients with PSC are men, and the diagnostic peak age of this disease is around 30–40 (12). Mayo Clinic has defined the four stages of PSC: Stage 1 is characterized by inflammation limited to the portal triad, with little or no periportal inflammation and fibrosis; Stage 2 is characterized by enlargement of portal tracts, and periportal fibrosis with or without periportal inflammation; Stage 3 is characterized by extension of septal fibrosis with or without bridging necrosis; and Stage 4 is characterized by biliary cirrhosis (13-15). Unfortunately, there is currently no effective therapy for end-

stage PSC that affects mortality other than liver transplantation. The yearly cost of all liver transplantation duo to PSC is approximately $125 million in the United States (16). Although ursodeoxycholic acid (UDCA) can improve liver biochemistry and surrogate prognostic markers, its use has not demonstrated a beneficial effect on patient survival (17). However, regulation of biliary fibrosis, especially in the histologic pre-cirrhotic stage, has been thought to be a promising therapeutic strategy for slowing the progression of PSC to the development of end-stage liver disease and cirrhosis (18).

Hepatic Inflammation

One hallmark of cholangiopathy is hepatic inflammation resulting from liver damage. Besides the secretion of pro-inflammatory factors, cholangiocytes are also involved in crosstalk and recruitment of immune cells, including neutrophils, macrophages, T lymphocytes, and dendritic cells. (7). As one of the most studied cell types in hepatic inflammation, heterogenous macrophages (consisting of resident Kupffer cells and infiltrating bone marrow-derived macrophages, BMDMs) play major roles in liver homeostasis, in the initiation of innate immune response to liver injury, but also in resolution of fibrosis and inflammation (19, 20). In the initial stage of hepatic injury, the damaged cholangiocytes and/or hepatocytes release danger-associated molecular patterns (DAMPs), such as high-mobility group protein B1 and IL-33 (21). DAMPs activate Kupffer cells that localize within the lumen of the liver sinusoids, which secrete pro-inflammatory cytokines such as TNF-α, IL-1β, and contribute to the activation of HSCs and scar formation (20). On the other hand, increased levels of C-C Motif Chemokine Ligand 2 (CCL2) promote the recruitment of BMDMs into the liver, which further

enhance the myofibroblast pool and fibrogenesis (22). Interestingly, Ly-6C^{hi} macrophages can acquire a restorative phenotype, with low expression of Ly-6C, which induces the degradation of extracellular matrix by metalloproteinases (MMPs) and myofibroblast apoptosis (19, 20). Although Kupffer cells and BMDMs share similar characteristics, freshly infiltrating BMDMs are CD11b^{hi}F4/80^{+} cells, whereas Kupffer cells are CD11b^{lo}F4/80^{hi} (23, 24).

Ductular Reaction

Ductular reaction is associated with various liver diseases, including cholangiopathies. It has been recognized as the proliferation of reactive bile ducts or hyperplasia and can be identified by expression of markers associated with cholangiocytes (25, 26). However, ductular reaction is not described solely as ductular proliferation because it comprises reactions associated not only with reactive cholangiocytes, but also other liver cells, including inflammatory cells (macrophages and lymphocytes), hepatic progenitor cells, mesenchymal cells and their corresponding signals (26, 27). With regards to cholangiopathies, extensive ductular reaction (expanded CK19^{+}, EpCAM^{+} and OV6^{+} cells) has been observed in human PSC or PBC liver tissues when compared to healthy controls (28).

Liver Fibrosis

Liver fibrosis is a reversible wound healing response, which is associated with excessive accumulation of extracellular matrix proteins, including collagens and fibronectin. Advanced liver fibrosis will lead to cirrhosis, which becomes irreversible and can eventually develop into liver cancer (29). HSCs are mesenchymal cells and have been

identified as the major extracellular matrix- (ECM-) producing cells in the injured liver. During healthy conditions, quiescent HSCs reside in the space of Disse, serving as storehouses of vitamin A. During liver injury, hepatic inflammation and ductular reaction triggers the activation of HSCs via the release of pro-fibrotic cytokines, such as TGF-β1 (30). Activated HSCs acquire a contractile, proinflammatory, and fibrogenic myofibroblast-like cell type and secrete large amounts of ECM proteins (31). In addition, during the resolution of liver fibrosis, MMP activities are increased and partial ECM degradation occurs, which is associated with the deactivation of HSC via apoptosis or senescence signaling pathways (32).

Biliary Senescence

Cellular senescence is a cell cycle arrest of proliferation that occurs when cells experience cellular stress, including DNA damage, dysfunctional telomeres and oncogenic mutations (33). Cellular senescence of cholangiocytes and the associated secretion of markers of senescence-associated secretory phenotypes (SASPs, e.g., TGF-β1, p16, CCL2 and SA-β-gal) are key hallmarks of cholangiopathies, and contribute to the paracrine activation of HSCs (coupled with decreased HSC senescence) and enhanced liver fibrosis (34-36). Furthermore, a large percentage of cholangiocytes in human PSC patients have been shown to exhibit SASPs (34, 36, 37).

Mdr2 Deficient Mice

Mdr2 (also known as Abcb4) is a mouse ortholog of the human multidrug resistance protein 3 (MDR3) gene encoding for the canalicular phospholipid transporter. Under healthy conditions, Mdr2 translocates phosphatidylcholine from the inner leaflet to

the outer leaflet of the membrane and subsequently forms mixed phospholipid-bile acid micelles (38, 39). Genetic disruption of the Mdr2 gene in mice causes: (i) the absence of phosphatidylcholine from bile; (ii) altered tight junction and leakage of toxic bile acids into portal tract; and (iii) intrahepatic induction of proinflammatory and profibrotic cytokines (e.g., TGF-β1, IL-1β, TNF-α) that spontaneously induce periductal inflammation and fibrosis (40). Because $Mdr2^{-/-}$ mice mimic the key characteristics of PSC, these mice have been considered as a promising *in vivo* model to study the pathogenesis of PSC (41-43).

Epithelial-mesenchymal Transition (EMT)

Epithelial-mesenchymal transition (EMT) is an event by which epithelial cells lose their native characteristics and display functional properties of mesenchymal cells (44). Recent studies show that EMT plays an important role in the development and progression of liver fibrosis. Immunostaining of liver sections from patients with cholangiopathies demonstrated a loss of epithelial markers, including E-cadherin, and the acquisition of S100a4 (the human homologue of fibroblast-specific protein-1) and other mesenchymal markers in cholangiocytes within fibrotic portal tracts (45-47). Interestingly, the concept of EMT has become one of the most controversial issues in liver fibrosis research (48, 49). As most studies supporting the occurrence of EMT in cholangiocytes are based essentially on a morphological approach, results from two linage tracing studies show evidence against the concept of cholangiocyte EMT in bile duct ligated (BDL) and carbon tetrachloride (CCl_4) models of fibrosis (50, 51). However, lineage tracing studies using

Cre-LoxP system also have some pitfalls. The efficiency of Cre-mediated recombination is not 100%. It is theoretically possible that mesenchymal transition might have occurred in the non-labeled cells.

Vimentin

Vimentin is a type III intermediate filament that has been found in various types of mesenchymal cells during different developmental stages (52, 53). The importance of intermediate filaments in regulating physiological properties of cells is becoming widely recognized in functions ranging from cell motility to signal transduction (52, 53). Induction of vimentin in epithelial cells results in several important features of EMT, including the adoption of a mesenchymal shape, loss of desmosomes, and increased focal adhesion and cell motility. Furthermore, when vimentin organization is altered or silenced in mesenchymal cells, those cells exhibit reduced motility and adopt an epithelial-like shape (53). It has been shown that vimentin is associated with cancer invasion and poor prognosis in numerous types of cancers, including breast cancer, prostate cancer, melanoma, and lung cancer, and serves as a potential target for cancer therapy (54, 55). Although vimentin expression has been found in liver cells that undergo EMT, the precise role of vimentin in the regulation of liver fibrosis is undefined.

Secretin and Secretin Receptor

Proliferating cholangiocytes secrete and respond to neuroendocrine hormones including secretin (Sct), which is produced by S cells of the duodenum, as well as cholangiocytes (56-58). In addition to stimulating biliary bicarbonate secretion by

interaction with basolateral secretin receptors (SR) expressed only by cholangiocytes (3, 56, 59, 60), the Sct/SR axis plays a key role in the modulation of biliary mass and liver fibrosis by both autocrine/paracrine mechanisms (8, 57, 58). For example, the activation of the Sct/SR axis increases: (i) intrahepatic biliary mass by microRNA 125b-dependent increased expression of vascular endothelial growth factor-A (VEGF-A) (58); and (ii) liver fibrosis by enhanced secretion of biliary TGF-β1 leading to paracrine activation of hepatic stellate cells (HSCs) (8). Conversely, knockout of SR or administration of a SR antagonist (Sct 5-27) inhibits ductular reaction and ameliorates liver fibrosis in bile duct ligated and $Mdr2^{-/-}$ mice (8, 57, 58). Furthermore, enhanced expression of the Sct/SR axis has been demonstrated in the liver of PSC patients compared to healthy individuals (8). Based on these previous findings about the characteristics and progression of cholestatic liver diseases, as well as the promising roles of Sct/SR and vimentin in ameliorating the liver damage, we proposed two specific aims: (i) to characterize the role of vimentin in the pathogenesis of biliary damage and liver fibrosis in PSC; (ii) to explore the effects of knockout of SR in $Mdr2^{-/-}$ mice on ductular reaction, EMT, cellular senescence and liver fibrosis. These studies provide new evidence that inhibition of vimentin or Sct/SR during cholestatic liver injury generates a response that seeks to counteract the enhanced ductular reaction, biliary senescence and liver fibrosis. Modulation of vimentin or Sct/SR expression may be a novel therapeutic option in the treatment of cholangiopathies including PSC.

CHAPTER II

MATERIALS AND METHODS

Materials

Reagents were purchased from Sigma Chemical Co. (St. Louis, MO) unless otherwise stated. Cell culture reagents and media were obtained from Invitrogen Corporation (Carlsbad, CA). The antibodies against α-SMA, Col1a1, desmin, E-cadherin, HNF4α, IL-6, p16, PCNA, TNF-α and vimentin were purchased from Abcam (Burlingame, CA); F4/80 and vimentin antibodies were obtained from Cell Signaling (Denver, MA); cytokeratin-19 (CK-19) antibody was purchased from Developmental Studies Hybridoma Bank (Iowa City, IA); and secretin receptor (SR) antibody was obtained from Bioss (Woburn, MA). Enzyme-linked immunosorbent assay (ELISA) kits to measure transforming growth factor-β1 (TGF-β1) levels in serum and cholangiocyte supernatant were purchased from Abcam (Burlingame, CA). Mouse Cytokine ELISA Plate Array I to measure inflammatory cytokines was purchased from Signosis (Santa Clara, CA). LY2109761, a TGF-β1 receptor antagonist, was obtained from Cayman Chemical (Ann Arbor, MI). RNA was extracted using the mirVana miRNA Isolation Kit from ThermoFisher Scientific and reverse transcribed with the iScript cDNA Synthesis Kit from Bio-Rad (Hercules, CA). All primer information for *q*PCR is listed in Table 1.

Table 1: List of *q*PCR primers.

Gene	Species	Detected transcript	Source
α-SMA	Mouse	NM_007392	QIAGEN
CCL2	Mouse	NM_011333	QIAGEN
Col1a1	Mouse	NM_007742	QIAGEN
E-cadherin	Mouse	NM_009864	QIAGEN
Fn1	Mouse	NM_010233	QIAGEN
GAPDH	Mouse	NM_008084	QIAGEN
IL-1β	Mouse	NM_008361	QIAGEN
IL-6	Mouse	NM_031168	QIAGEN
Ki67	Mouse	NM_001081117	QIAGEN
N-cadherin	Mouse	NM_007664	QIAGEN
PCNA	Mouse	NM_011045	QIAGEN
p16	Mouse	NM_009877	QIAGEN
p21	Mouse	NM_007669	QIAGEN
S100a4	Mouse	NM_011311	QIAGEN
TGF-β1	Mouse	NM_011577	QIAGEN
TNF-α	Mouse	NM_013693	QIAGEN
vimentin	Mouse	NM_011701	QIAGEN
α-SMA	Human	NM_001141945	QIAGEN
CCL2	Human	NM_002982	QIAGEN

Table 1 Continued List of *q*PCR primers.

Gene	Species	Detected transcript	Source
Col1α1	Human	NM_000088	QIAGEN
E-cadherin	Human	NM_ 004360	QIAGEN
Fn-1	Human	NM_002026	QIAGEN
GAPDH	Human	NM_001256799	QIAGEN
N-cadherin	Human	NM_001042572	QIAGEN
p16	Human	NM_000077	QIAGEN
p21	Human	NM_000389	QIAGEN
S100a4	Human	NM_002961	QIAGEN
TGF-β1	Human	NM_000660	QIAGEN
vimentin	Human	NM_003380	QIAGEN

Animal Models

All animal procedures were performed in accordance with protocols approved by the Baylor Scott & White Institutional Animal Care and Use Committee (IACUC). FVB/NJ mice (WT control for $Mdr2^{-/-}$ mice) and $Mdr2^{-/-}$ mice were originally purchased from Jackson Laboratories (Bar Harbor, ME); C57BL/6 mice (WT control for $SR^{-/-}$ mice) were purchased from Charles River (Wilmington, MA); C57/FVB mice were obtained after breeding C57BL/6 with FVB/NJ mice; the colonies of these corresponding control mice were established in our animal facility (8, 57). The established mouse strains having different backgrounds, $SR^{-/-}$ and $Mdr2^{-/-}$, were crossed until the homozygous double knockout ($SR^{-/-}/Mdr2^{-/-}$) mice were obtained. The genotype of each $SR^{-/-}/Mdr2^{-/-}$ mouse was confirmed by PCR amplification of genomic DNA extracted from the tail. To assess the *in vivo* inhibitory effect of vimentin, $Mdr2^{-/-}$ mice (n=6) were treated with Vivo-Morpholino sequences of vimentin (5'-ACACAGACCTGGTAGACATGGCTTC-3') or mismatched Morpholino (5'-ACAGACACCTCGTACACATCGCTTC-3') (Gene Tools LCC, Philomath, OR) delivered by two tail vein injections 1 week apart (30 mg/kg BW) (58, 61). All mice were housed in a temperature-controlled environment (20-22°C) with 12:12-hr light-dark cycles and fed ad libitum standard chow with free access to drinking water. Before liver perfusion, these mice (all 12 weeks of age) were euthanized with Euthasol™ (200-250 mg/kg BW, i.p.) (8, 62). In all groups, serum, liver tissues and cholangiocytes were collected; liver weight, body weight and liver/body weight ratio (an index of liver cell growth) were measured/calculated (56).

Isolation of Mouse Cholangiocytes and HSCs

Mouse cholangiocytes were isolated as described using a monoclonal IgG2a antibody against an unidentified membrane antigen expressed by all intrahepatic cholangiocytes (provided by R. Faris, Brown University, Rhode Island, RI) (3, 63, 64). Cell number and viability (≥99%) were assessed by trypan blue exclusion (65). Cholangiocyte (1 million cells/100 μl) supernatants were collected after short-term incubation with 0.1 M calcium chloride ($CaCl_2$) at 37°C for 4-6 h (8, 66, 67).

Mouse HSCs were isolated by laser capture microdissection (LCM). Frozen liver sections (10-μm thick) were incubated overnight with an antibody specific for desmin (marker of stellate cells) (68-70). Following staining, desmin-positive HSCs were dissected from the slides using the Leica LMD7000 (Buffalo Grove, IL) laser dissection microscope and collected into a PCR tube before being analyzed. The RNA from HSCs was extracted with the Arcturus PicoPure RNA isolation kit from Thermo Fisher Scientific (Mountain View, CA).

Evaluation of EMT in Animal Models

We measured: (i) immunoreactivity of vimentin and other EMT markers (E-cadherin and S100a4) in liver sections by immunohistochemistry and/or immunofluorescence performed in conjunction with staining for a cholangiocyte marker (CK-19) or HSC marker (desmin); and (ii) expression of mesenchymal markers (N-cadherin and S100a4) by qPCR in isolated cholangiocytes. The *q*PCR was performed

using RT2 SYBR Green/ROX quantitative PCR master mix with the Applied Biosystems ViiA7 real-time PCR system (Carlsbad, CA) according to the manufacturer's protocol.

Assessment of Liver Damage

Liver histology was evaluated in paraffin-embedded liver sections (4-μm thick) stained with hematoxylin and eosin (H&E). Observations were processed in a blinded fashion by a board-certified pathologist. The serum levels of glutamic oxaloacetic (SGOT), glutamate pyruvate transaminase (SGPT) and alkaline phosphatase (ALP) were measured using an IDEXX Catalyst One Chemistry Analyzer and VetLab Station (Westbrook, ME). Intrahepatic bile duct mass (IBDM) was evaluated in formalin-fixed, paraffin-embedded (FFPE) liver sections (4-5 μm thick, 10 different fields analyzed for each sample from 3 different animals) by immunohistochemistry for CK-19. IBDM was calculated as the area occupied by CK-19-positive bile ducts/total area using VisioPharm software (Westminster, CO). Sections were examined using Olympus cellSens software (Japan). Biliary proliferation was evaluated by measurement of PCNA and Ki67 expression in cholangiocytes by immunoblots and/or qPCR.

Measurement of Liver Fibrosis

Liver fibrosis was assessed by Sirius Red staining in FFPE liver sections (4-5 μm thick). Collagen content was examined using the Olympus cellSens software and quantified using VisioPharm software. Immunofluorescence staining was performed for Col1a1 co-stained for CK-19 and/or desmin in frozen liver sections (8-10 μm thick).

Immunofluorescent staining was visualized using the Leica TCS SP5 X system, or the Olympus Fluoview confocal microscopes located in the Texas A&M Integrated Microscopy and Imaging Laboratory. The expression of profibrotic markers (Col1a1, Fn1 and TGF-β1) was evaluated in cholangiocytes, HSCs or total liver lysates by *q*PCR and/or immunoblots. TGF-β1 levels were also measured in serum and cholangiocyte supernatants by ELISA.

Evaluation of Biliary Senescence

Biliary senescence was evaluated in frozen liver sections (10-μm thick) by: (i) staining for senescence-associated-β-galactosidase (SA-β-gal) using a cellular senescence assay kit (MilliporeSigma, Billerica, MA); and (ii) immunofluorescence for p16 (co-stained for CK-19). SA-β-gal staining was quantified as the area occupied by SA-β-gal-positive bile ducts/total area using VisioPharm software. The expression of senescence genes (p16 and p21) was evaluated in purified cholangiocytes and LCM-isolated HSCs by *q*PCR.

Measurement of Hepatic Inflammation

Hepatic inflammation was evaluated in FFPE liver sections (4-5 μm thick) by immunohistochemistry for F4/80. Sections were examined using the Olympus cellSens software. Quantitative analysis of staining was performed using VisioPharm software. The expression of proinflammatory markers (IL-1β, IL-6 and TNF-α) was evaluated in cholangiocytes or total liver lysates by *q*PCR and/or immunoblots.

Evaluation of EMT in Human Control and PSC Patients

Coded human liver specimens were obtained through the Liver Tissue Procurement and Distribution System (Minneapolis, MN) as described previously (71). In addition, liver tissues from patients with end stage PSC were obtained from the explant generated during liver transplantation. Control liver samples were from patients with no known history of chronic liver diseases and collected during abdominal surgeries for various unrelated causes. The study protocol to obtain liver tissues was approved by the Institutional Review Board at Indiana University-Purdue University Indianapolis. The sources of the human samples are shown in Table 2. The expression of vimentin and other EMT markers was evaluated by *q*PCR, immunohistochemistry, immunofluorescence or immunoblots in control and PSC patients. Protein expression was normalized to GAPDH and quantified using the LI-COR Image Studio software (Lincoln, NE).

Table 2: Characteristics of human control and PSC samples.

Group	No.	Diagnosis	Age	Gender	Ethnicity	Sample Type
Control	S1	Normal	N/A	N/A	N/A	Total liver
Control	S2	Normal	N/A	N/A	N/A	Total liver
Control	S3	Normal	N/A	N/A	N/A	Total liver
Control	S4	Normal	N/A	N/A	N/A	Total liver
Control	S5	Normal	N/A	N/A	N/A	Total liver
Control	S6	Normal	N/A	N/A	N/A	FFPE liver sections
PSC	S1	Late stage PSC	60	Male	Caucasian	Total liver
PSC	S2	Early stage PSC	N/A	N/A	Caucasian	Total liver
PSC	S3	Early stage PSC	57	Male	Caucasian	Total liver
PSC	S4	Early stage PSC	33	Male	Caucasian	Total liver

Table 2 Continued: Characteristics of human control and PSC samples.

Group	No.	Diagnosis	Age	Gender	Ethnicity	Sample Type
PSC	S5	Early stage PSC	47	Female	Caucasian	Total liver
PSC	S6	Early stage PSC	42	Male	Caucasian	Total liver
PSC	S7	Early stage PSC	63	Male	Caucasian	Total liver
PSC	S8	Stage I PSC	N/A	N/A	N/A	FFPE liver sections
PSC	S9	Stage IV PSC	N/A	N/A	N/A	FFPE liver sections

FFPE = formalin fixed paraffin embedded; N/A = Not available; PSC = Primary Sclerosing Cholangitis.

In Vitro Studies in HIBEpiCs, hPSCL and HHSteCs

The *in vitro* studies were performed in the following cell lines: human intrahepatic biliary epithelial cells (HIBEpiCs, ScienCell, Carlsbad, CA), human PSC patient-derived cholangiocytes (hPSCL, a gift from N. LaRusso, Mayo Clinic, Rochester, MN), and human hepatic stellate cells (HHSteCs, ScienCell, Carlsbad, CA). The expression of vimentin was evaluated by immunofluorescence in hPSCL cells and HIBEpiCs (control for hPSCL). To examine the impact of vimentin in epithelial mesenchymal crosstalk, HIBEpiCs were seeded on six-well plates to approximately 60% to 70% confluence in complete medium containing 5% fetal bovine serum and then changed to reduced-serum (2%) medium with control or vimentin CRISPR/Cas9 KO plasmid transfection (Santa Cruz, Dallas, TX), according to the manufacturer's protocol. After 24 hours, recombinant human TGF-β1 (R&D System, Minneapolis, MN) was added to the culture at a final concentration of 2.5 ng/ml to induce mesenchymal transition (72, 73). The cells were incubated for 72 hours before harvesting and subjected to *q*PCR experiments as described below. In basal HIBEpiCs and control or vimentin CRISPR/Cas9 KO plasmid-transfected HIBEpiCs with/without TGF-β1 stimulation, we measured the mRNA expression of EMT markers (vimentin and E-cadherin), fibrotic markers (Col1a1 and Fn1) and senescence markers (p16 and p21) by *q*PCR.

HHSteCs were incubated for 12 hr at 37°C with (i) cholangiocyte supernatant from all groups of mice; and (ii) cholangiocyte supernatant from $Mdr2^{-/-}$ mice in the absence or presence of LY2109761 (10 μM), a TGF-β1 receptor antagonist, before measuring the

expression of E-cadherin, fibrotic markers (Col1a1, Fn1 and TGF-β1) and senescence markers (p16 and p21) by *q*PCR (8, 74).

Measurement of Secretin and Secretin Receptor

The immunoreactivity of SR was measured by immunohistochemistry in paraffin-embedded liver sections (4-5 μm thick, 10 different fields analyzed for each sample from 3 different animals). Sct levels were measured in serum and cholangiocyte supernatants using ELISA kits (Phoenix Pharmaceuticals, Inc., Burlingame, CA).

Evaluation of microRNA 125b

Isolation of miRNAs was performed in isolated cholangiocytes using the mirVana miRNA Isolation Kit from ThermoFisher Scientific (Waltham, MA). Single stranded cDNA was synthesized from 1 μg of RNA from the aforementioned samples using the TaqMan microRNA reverse transcription kit (Applied Biosystems, Waltham, MA) and was amplified by quantitative PCR (*q*PCR) using sequence-specific primers from the TaqMan microRNA Assays on an Applied Biosystems Viia7 Real-Time PCR System (Thermo Fisher Scientific; Waltham, MA), according to the manufacturer's protocol.

Ingenuity Pathway Analysis (IPA) Software

The genes related to senescence and fibrosis were analyzed using Ingenuity Pathway Analysis (IPA) software (Qiagen, Redwood City, CA) for the functionally relevant pathway (75, 76). IPA is a web-based functional analysis software that helps

researchers to search for targeted information on genes, proteins, chemicals, diseases, and drugs, as well as building custom biological models in life science research.

Statistical Analysis

All data are expressed as the mean ± SEM. Differences between groups were analyzed by Student's unpaired t-test when two groups were analyzed or one-way ANOVA (followed by an appropriate post hoc test) when more than two groups were analyzed. A value of $p<0.05$ was utilized to indicate statistically significant differences.

CHAPTER III

RESULTS

Enhanced Vimentin Expression in Mdr2$^{-/-}$ Mice

By immunohistochemistry and/or immunofluorescence in liver sections from WT and Mdr2$^{-/-}$ mice, we observed enhanced immunoreactivity of vimentin in the periductal area from Mdr2$^{-/-}$ compared to WT mice (Figure 1a-b). Interestingly, although CK-19-positive cholangiocytes were surrounded by vimentin-positive cells, no merging signals between vimentin and CK-19 were observed.

Vimentin Expression was Reduced with the Vimentin Vivo-Morpholino Treatment

To evaluate the role of vimentin in the pathogenesis of cholestatic liver injury, we performed treatments aimed to reduce the hepatic expression of vimentin in Mdr2$^{-/-}$ mice. In Mdr2$^{-/-}$ mice treated with vimentin Vivo-Morpholino, there was a significant decrease in vimentin expression compared to Mdr2$^{-/-}$ mice treated with mismatch-Morpholino. No significant differences were observed between Mdr2$^{-/-}$ mice and Mdr2$^{-/-}$ mice treated with mismatch-Morpholino (Figure 1a-b).

Effects of Vimentin Vivo-Morpholino Treatment on Other EMT Markers

We then evaluated the expression of other EMT markers to see the effect of vimentin knockdown. By immunofluorescence for CK-19 with another commonly used mesenchymal marker, S100a4, we observed enhanced immunoreactivity of S100a4 in the

periductal area from Mdr2$^{-/-}$ compared to WT mice, which was reduced in Mdr2$^{-/-}$ mice treated with vimentin Vivo-Morpholino (Figure 2a). Interestingly, there was a significant reduction in N-cadherin and S100a4 expression in cholangiocytes from Mdr2$^{-/-}$ mice treated with vimentin Vivo-Morpholino compared to Mdr2$^{-/-}$ and Mdr2$^{-/-}$ mice treated with mismatched vimentin Vivo-Morpholino (Figure 2b). In addition, by immunofluorescence in liver sections, we observed a reduction of E-cadherin immunoreactivity (co-localized with CK-19) in Mdr2$^{-/-}$ mice compared with WT mice (Figure 2c). However, there was enhanced E-cadherin expression in Mdr2$^{-/-}$ mice treated with vimentin Vivo-Morpholino (Figure 2c).

Effects of Vimentin Vivo-Morpholino Treatment on HSCs

Previous studies have shown that quiescent HSCs are capable of transdifferentiation into myofibroblast-like cells during the progression of liver fibrosis and that they gain a mesenchymal phenotype (31, 77). We also evaluated the expression change of E-cadherin and vimentin in HSCs by co-staining for desmin, the HSC marker (68-70). With the treatment of vimentin Vivo-Morpholino, we observed less co-expression of desmin/vimentin and increased co-localization of desmin/E-cadherin compared to Mdr2$^{-/-}$ mice, indicating the HSCs are less myofibroblast-like with the knockdown of vimentin (Figure 3).

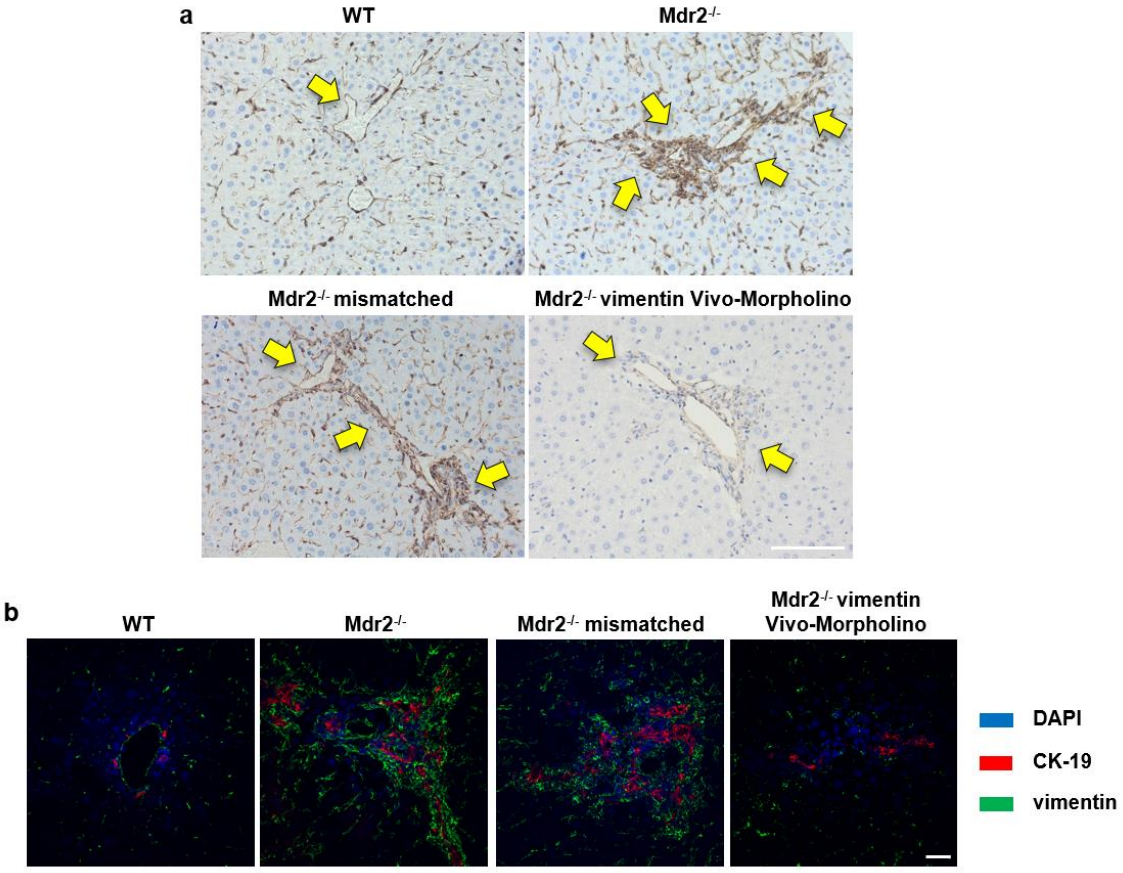

Figure 1: Evaluation of vimentin expression in liver sections. [a] Immunohistochemistry for vimentin in liver sections, original magnification 20X, scale bar = 100 μm. [b] Immunofluorescence for vimentin (in green) co-stained for CK-19 (in red). Nuclei are stained with DAPI. original magnification 40X, scale bar = 20 μm.

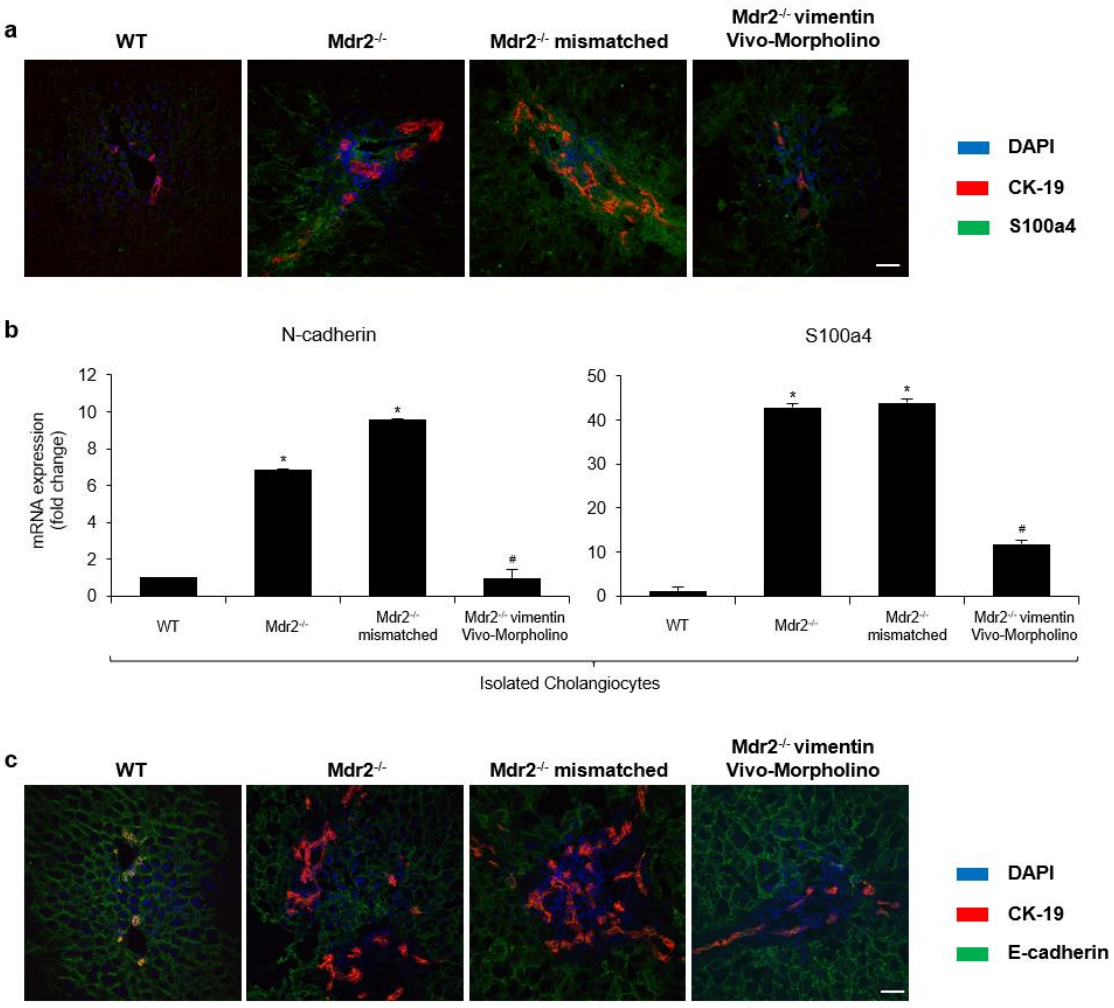

Figure 2: Evaluation of epithelial and mesenchymal phenotypes in cholangiocytes. [a] Immunofluorescence for S100a4 (in green) in liver sections co-stained for CK-19 (in red). Nuclei are stained with DAPI. Original magnification 40X, scale bar = 20 μm. [b] The mRNA expression of EMT markers was evaluated by *q*PCR in isolated cholangiocytes. *p<0.05 versus WT mice; #p<0.05 versus Mdr2$^{-/-}$ mice. [c] Immunofluorescence for E-cadherin (in green) in liver sections co-stained for CK-19 (in red). Nuclei are stained with DAPI. Original magnification 40X, scale bar = 20 μm.

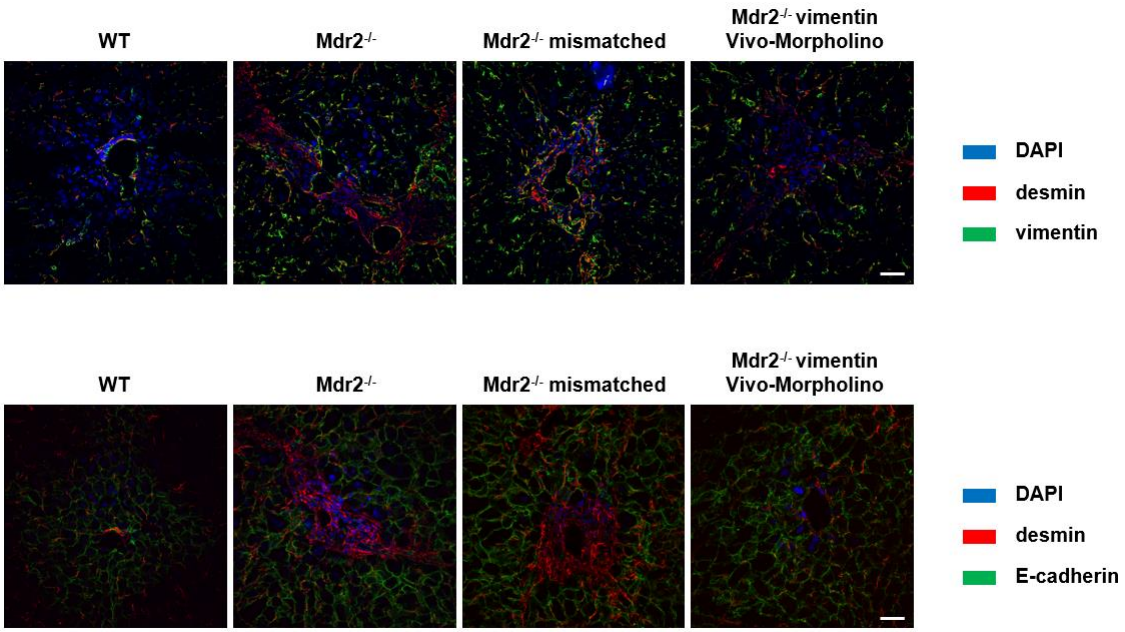

Figure 3: Evaluation of epithelial and mesenchymal phenotypes in HSCs. Immunofluorescence for vimentin or E-cadherin (in green) in liver sections co-stained for desmin (in red). Nuclei are stained with DAPI. Original magnification 40X, scale bar = 20 μm.

Knockdown of Vimentin Ameliorates Liver Damage

By H&E staining, histopathological changes indicative of liver damage were observed in Mdr2$^{-/-}$ compared to WT mice, which were ameliorated in Mdr2$^{-/-}$ mice treated with vimentin Vivo-Morpholino (Figure 4a). While liver sections of Mdr2$^{-/-}$ mice and Mdr2$^{-/-}$ mice treated with mismatched Vivo-Morpholino showed both early and focal complete portal-portal bridging fibrosis and moderate to marked ductular reaction, liver sections of Mdr2$^{-/-}$ mice treated with vimentin Vivo-Morpholino showed early portal-portal bridging fibrosis and mild ductular reaction. Interestingly, serum levels of SGOT, SGPT, and ALP were higher in Mdr2$^{-/-}$ compared with WT mice, but decreased in Mdr2$^{-/-}$ mice treated with vimentin Vivo-Morpholino compared to Mdr2$^{-/-}$ mice (Table 3). In addition, there was a significant increase in IBDM from Mdr2$^{-/-}$ mice compared to WT mice, which was reduced in Mdr2$^{-/-}$ mice treated with vimentin Vivo-Morpholino (Figure 4b); no significant changes in IBDM were observed between Mdr2$^{-/-}$ mice and Mdr2$^{-/-}$ mice treated with mismatched Vivo-Morpholino (Figure 4b).

Vimentin Morpholino Treatment Decreases Liver Fibrosis

Collagen deposition was increased in Mdr2$^{-/-}$ compared to WT mice but was significantly decreased in Mdr2$^{-/-}$ mice treated with vimentin Vivo-Morpholino compared to Mdr2$^{-/-}$ and Mdr2$^{-/-}$ mice treated with mismatched Vivo-Morpholino (Figure 5a). By immunofluorescence, there was enhanced immunoreactivity for Col1a1 in cholangiocytes and HSCs (co-stained for CK-19 and desmin, respectively) from Mdr2$^{-/-}$ compared to WT mice, immunoreactivity that was reduced in Mdr2$^{-/-}$ mice treated with vimentin Vivo-

Morpholino (Figure 5b). Furthermore, in isolated cholangiocytes, the expression of fibrosis markers (Col1a1, TGF-β1 and α-SMA) was significantly increased in Mdr2$^{-/-}$ compared to WT mice but decreased in Mdr2$^{-/-}$ mice treated with vimentin Vivo-Morpholino (Figure 5c). In addition, TGFβ-1 levels were significantly increased in serum and cholangiocyte supernatants collected from Mdr2$^{-/-}$ mice compared with WT mice but decreased in Mdr2$^{-/-}$ mice treated with vimentin Vivo-Morpholino (Table 3).

Knockdown of Vimentin Reduces Biliary Senescence

By SA-β-gal staining in liver sections, we found enhanced biliary senescence in Mdr2$^{-/-}$ compared with WT mice, which was significantly decreased in Mdr2$^{-/-}$ mice treated with vimentin Vivo-Morpholino (Figure 6a). There was enhanced immunoreactivity for p16 in cholangiocytes (co-stained with CK-19) from Mdr2$^{-/-}$ mice compared with WT mice, immunoreactivity that was reduced in Mdr2$^{-/-}$ mice treated with vimentin Vivo-Morpholino (Figure 6b). There was enhanced expression of p16 and p21 in cholangiocytes from Mdr2$^{-/-}$ mice compared to WT mice, which decreased in Mdr2$^{-/-}$ mice treated with vimentin Vivo-Morpholino (Figure 7a). Conversely, we observed decreased expression of p16 and p21 in LCM-isolated HSCs from Mdr2$^{-/-}$ mice, which was significantly elevated in Mdr2$^{-/-}$ mice treated with vimentin Vivo-Morpholino (Figure 7b).

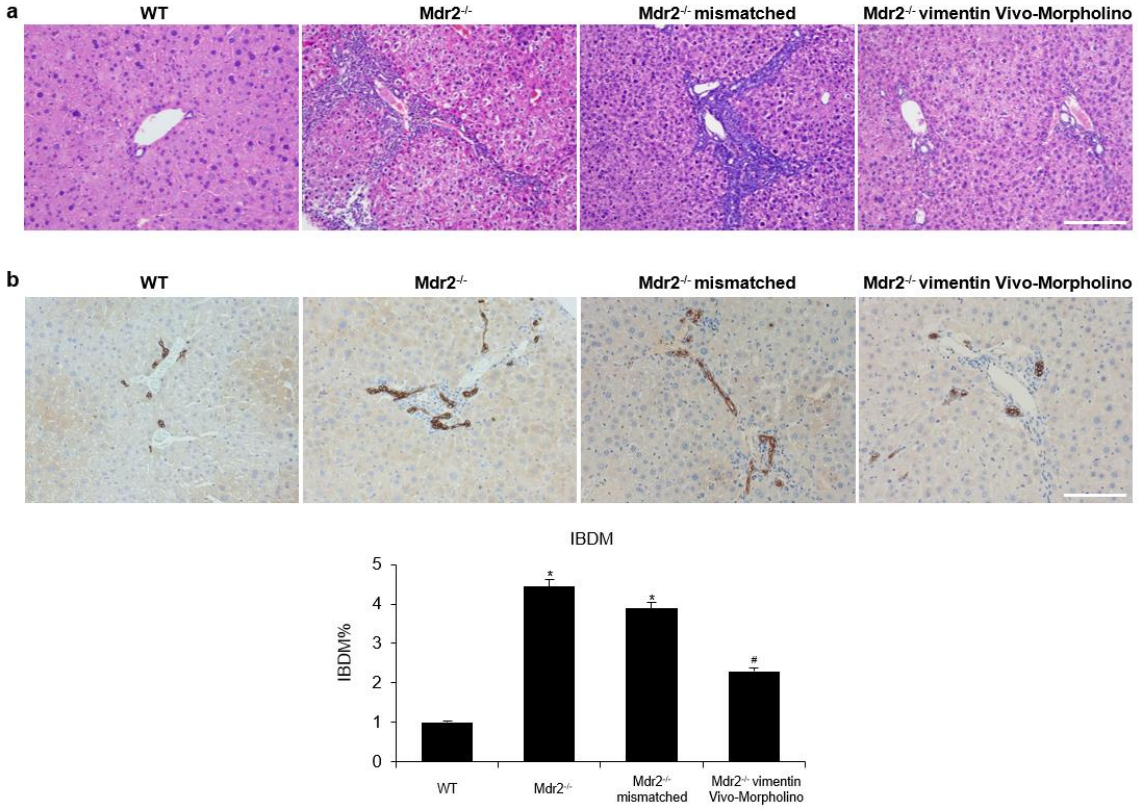

Figure 4: Knockdown of vimentin reduced liver damage, ductular reaction and intrahepatic bile duct mass (IBDM). [a] Liver histology was evaluated in liver sections (4-μm thick) stained with hematoxylin and eosin (H&E). Observations were processed in a blinded fashion by a board-certified pathologist. Original magnification 20X, scale bar = 100 μm. [b] Immunohistochemistry for CK-19 in liver sections, original magnification 20X, scale bar = 100 μm. [c] Percentage of IBDM. *$p<0.05$ versus WT mice; #$p<0.05$ versus $Mdr2^{-/-}$ mice.

Table 3: Liver and body weight, liver/body weight ratio, serum chemistry and TGF-β1 levels in Mdr2$^{-/-}$ vimentin Vivo-Morpholino-treated mice and relevant controls.

Parameters	WT	Mdr2$^{-/-}$	Mdr2 mismatched	Mdr2$^{-/-}$ vimentin morpholino
Liver weight (g)	2.0±0.5 n=6	2.9±0.3 n=6	3.2±0.2 n=4	2.7±0.4 n=6
Body weight (g)	30.2±1.7 n=6	29.5±2.1 n=6	31.7±1.8 n=4	29.6±1.2 n=6
Liver to body weight ratio (%)	6.9±1.6 n=6	9.7±1.1* n=6	10.2±0.1 n=4	9.2±1.0 n=6
SGOT (Units/L)	160.8±10.9 n=6	930.0±61.75* n=6	1013.8±95.4* n=4	528.8±32.6$^{\#}$ n=4
SGPT (Units/L)	538.3±57.2 n=6	1758.3±65.5* n=6	1363.8±102.3* n=4	862.5±154.1$^{\#}$ n=4
ALP (Units/L)	<50±0.0 n=6	271.7±10.3* n=6	347.5±27.6* n=4	140.0±6.1$^{\#}$ n=4
TGF-β1 levels in serum (ng/ml)	4.5±0.1 n=3	14.4±0.5* n=3	14.6±0.5* n=3	9.3±0.9$^{\#}$ n=3
TGF-β1 levels in cholangiocyte Supernatant (ng/ml)	1.3±0.1 n=3	3.1±0.0* n=3	2.6±0.1* n=3	1.0±0.1$^{\#}$ n=3

*P<0.05 vs. WT mice; $^{\#}$P<0.05 vs. Mdr2$^{-/-}$ mice.

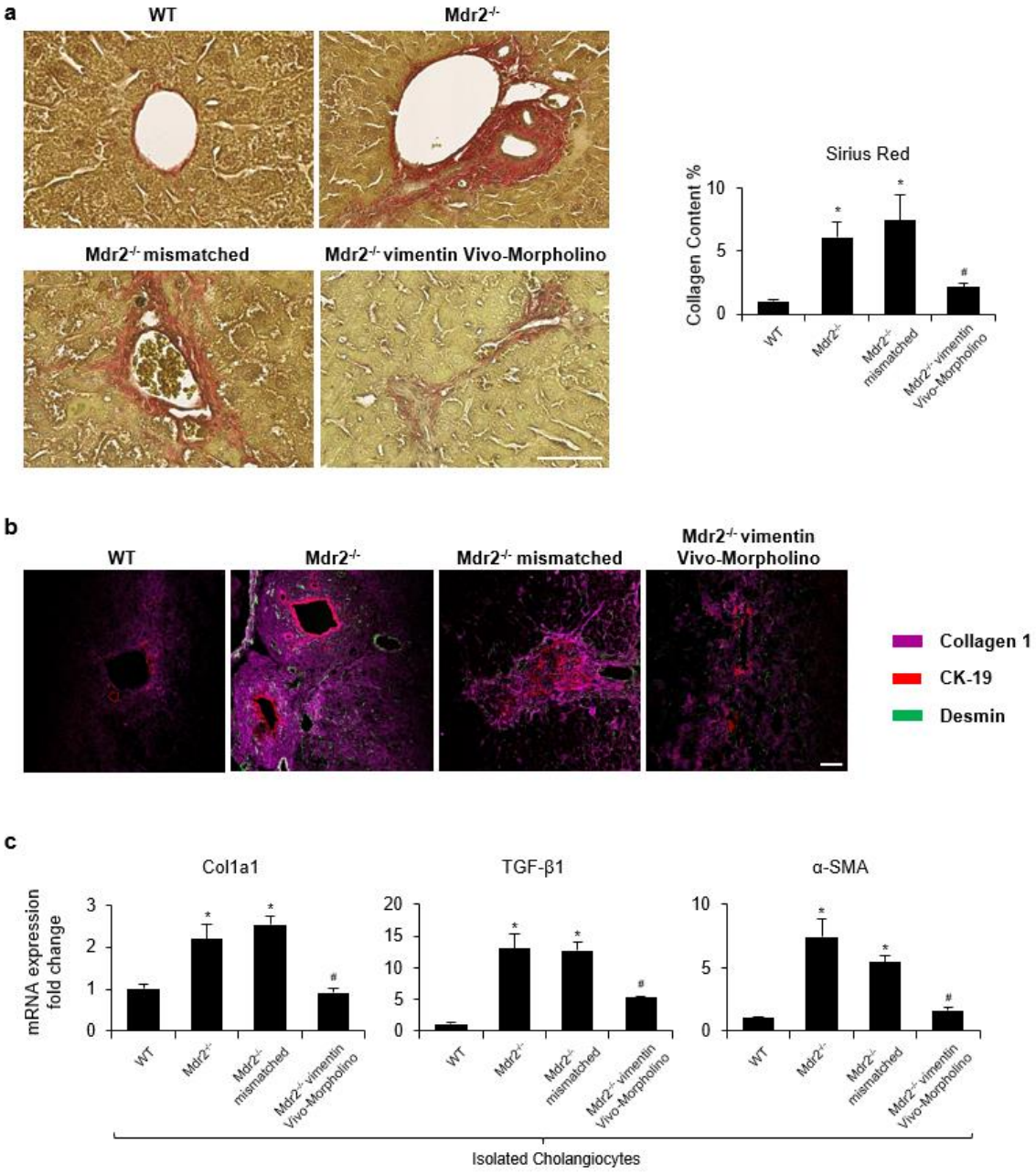

Figure 5: Knockdown of vimentin decreased liver fibrosis. [a] Measurement of collagen deposition by Sirius Red staining in liver sections. Orig. magnification 20X, scale bar = 100 μm. [b] Immunofluorescence for collagen 1 (in magenta) in liver sections co-stained for CK-19 (in red) and desmin (in green). Original magnification 40X, scale bar = 20 μm. [c] The mRNA expression of fibrotic markers was evaluated by *q*PCR in isolated cholangiocytes. *p<0.05 versus WT mice; #p<0.05 versus Mdr2$^{-/-}$ mice.

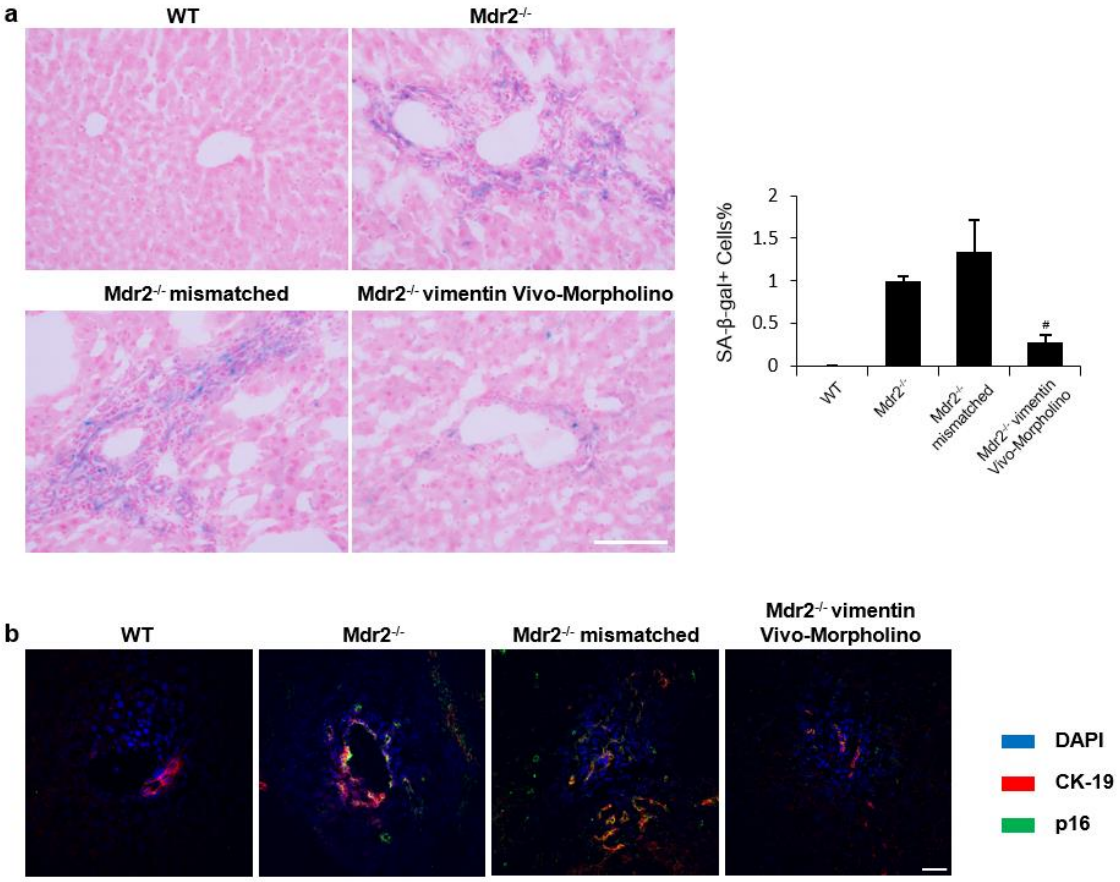

Figure 6: Knockdown of vimentin reduced biliary senescence. [a] Measurement of cellular senescence by SA-β-gal staining in liver sections, original magnification 20X, scale bar = 100 μm. Percentage of SA-β-gal-positive area. #p<0.05 versus Mdr2$^{-/-}$ mice. [b] Immunofluorescence for p16 (in green) in liver sections co-stained for CK-19 (in red). Nuclei are stained with DAPI. Original magnification 40X, scale bar = 20 μm.

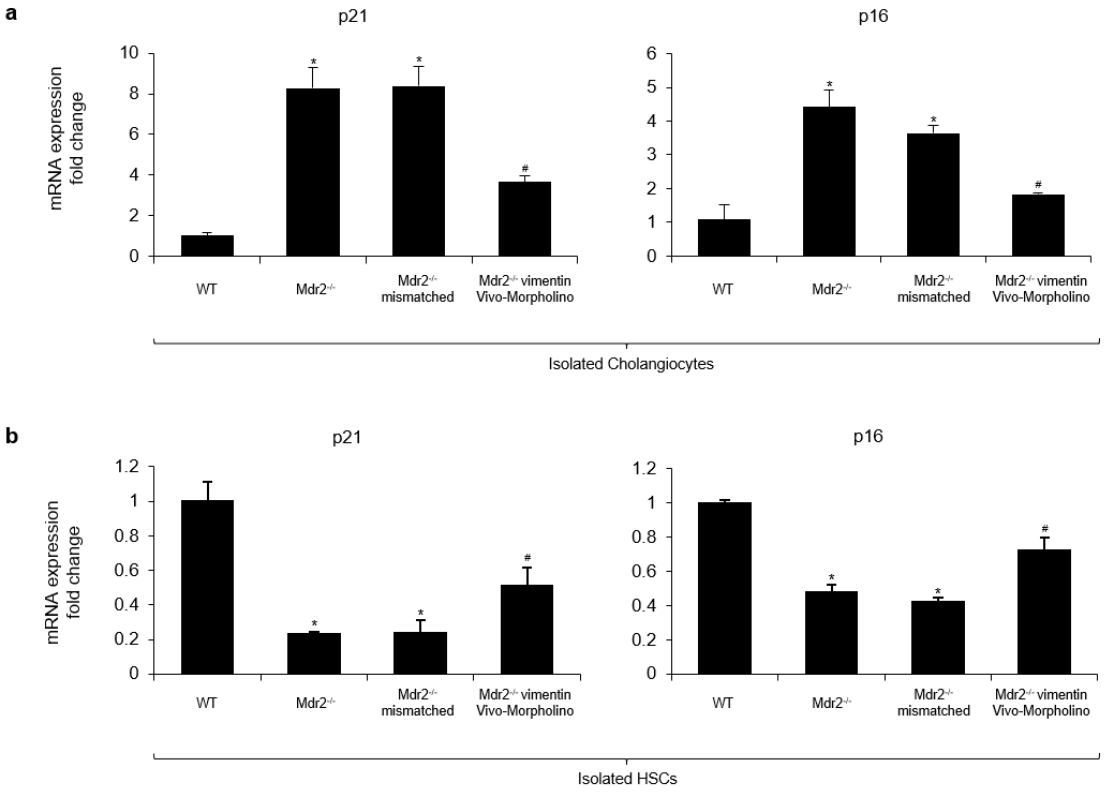

Figure 7: Expression of senescence markers in cholangiocytes and HSCs. The mRNA expression of senescence markers was evaluated by *q*PCR in isolated cholangiocytes and hepatic stellate cells (HSCs). *p<0.05 versus WT mice; #p<0.05 versus Mdr2$^{-/-}$ mice.

Vimentin Morpholino Treatment Decreases Hepatic Inflammation

As indicated by the immunohistochemistry for F4/80, knockdown of vimentin also reduced the macrophage population in livers of Mdr2$^{-/-}$ mice (Figure 8a). Furthermore, in isolated cholangiocytes, the expression of proinflammatory markers (IL-1β and IL-6) was significantly increased in Mdr2$^{-/-}$ compared to WT mice but decreased in Mdr2$^{-/-}$ mice treated with vimentin Vivo-Morpholino (Figure 8b).

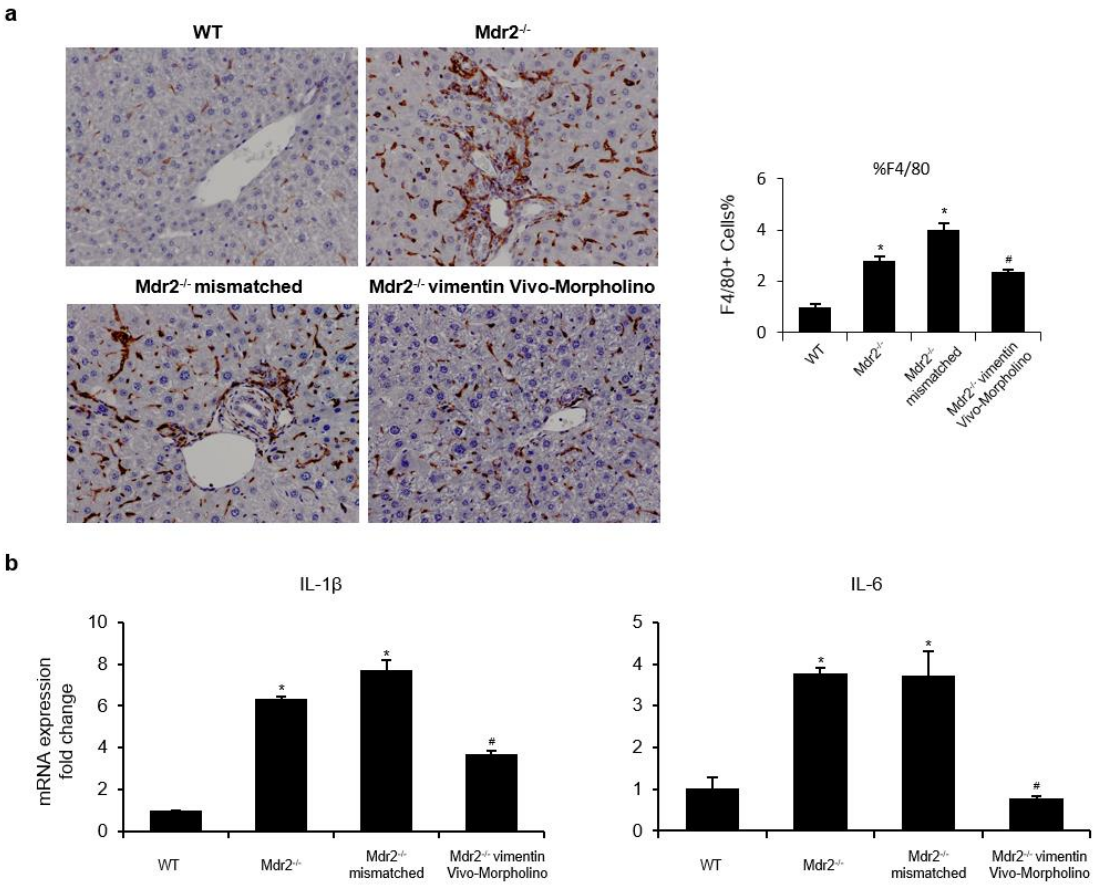

Figure 8: Evaluation of hepatic inflammation in liver sections. [a] Immunohistochemistry for F4/80 in liver sections, original magnification 20X, scale bar = 100 μm. Percentage of F4/80-positive area. *p<0.05 versus WT mice; #p<0.05 versus Mdr2$^{-/-}$ mice. [B] The mRNA expression of proinflammatory markers was evaluated by *q*PCR in isolated cholangiocytes. *p<0.05 versus WT mice; #p<0.05 versus Mdr2$^{-/-}$ mice.

Expression of EMT Markers in Human PSC Patients and Isolated PSC Patient-derived Cholangiocytes

By *q*PCR, we observed that the mRNA expression of vimentin and S100a4 was significantly higher in PSC patients compared to healthy controls, whereas the expression of E-cadherin and N-cadherin showed no significant differences in PSC patients compared with healthy controls (Figure 9a, Table 2). In addition, there was increased immunoreactivity of vimentin expression and decreased CK-19 staining intensity in liver sections from early stage PSC patients compared to healthy controls (Figure 9b). Upregulation of vimentin and CK-19 expression was significantly exacerbated in liver sections from late stage PSC patients (Figure 9b). Based on immunoblots, there were increased protein levels of vimentin, along with α-SMA and Col1a1 in PSC patients compared to healthy controls (Figure 10). However, there was no significant difference in E-cadherin expression between PSC patients and healthy controls (Figure 9-10). Morphological changes were observed with the staining of vimentin in hPSCL cells compared to HIBEpiCs (Figure 11). Staining for CK-19 and HNF4α was used to verify the purity of the cultured cells and to exclude contamination with hepatocytes (Figure 11).

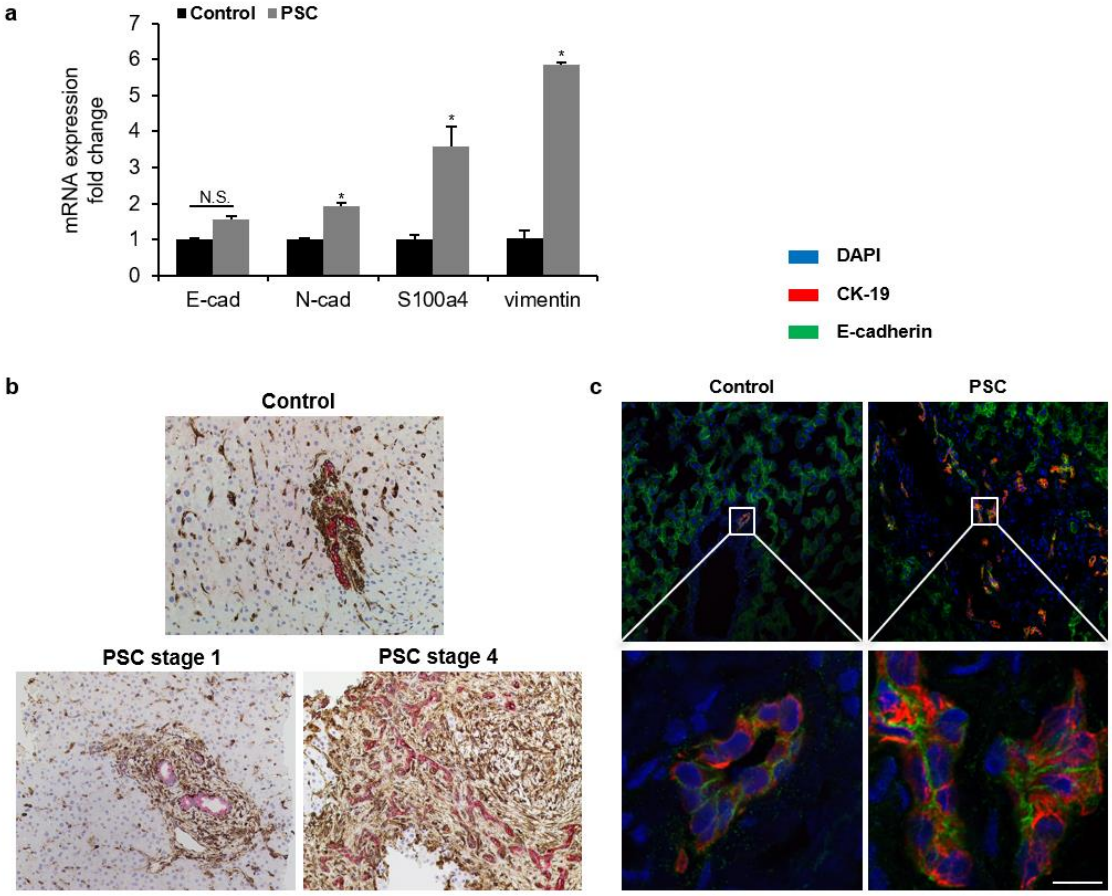

Figure 9: Expression of EMT markers in human PSC patients. [a] The mRNA expression of EMT markers was evaluated by *q*PCR in healthy controls and PSC patients. *p<0.05 versus healthy controls. [b] Immunohistochemistry for vimentin (in brown) in liver sections co-stained for CK-19 (in red) in human FFPE sections, original magnifcation 20X, scale bar = 100 μm. [c] Immunofluorescence for E-cadherin (in green) in liver sections co-stained with CK-19 (in red). Nuclei are stained with DAPI. Original magnification 20X, scale bar = 10 μm.

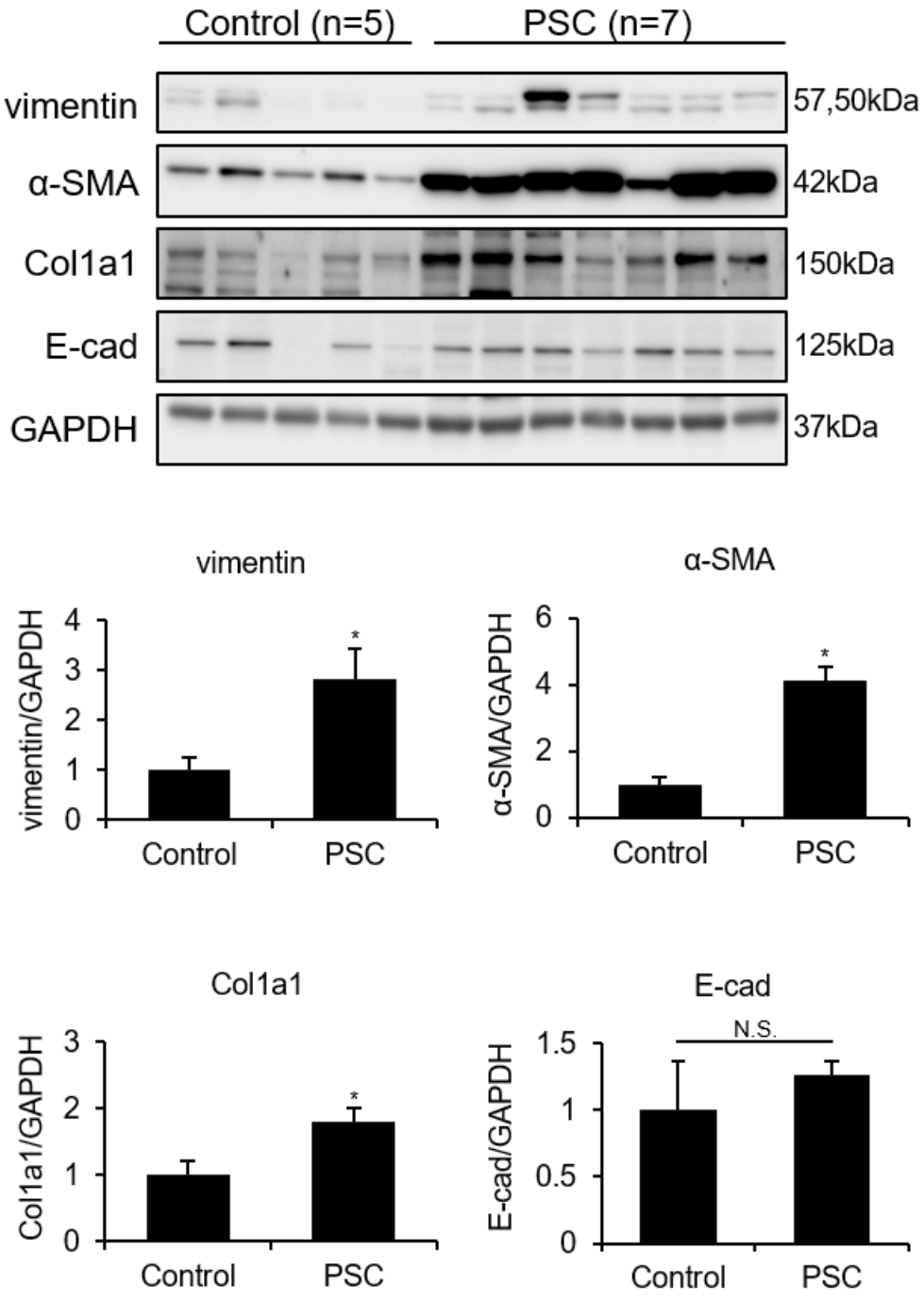

Figure 10: Protein levels of EMT and fibrotic markers in human PSC patients. Western blot analyses for EMT and fibrotic markers in healthy controls and PSC patients. Protein expression levels were normalized to GAPDH expression levels. *p<0.05 versus healthy controls.

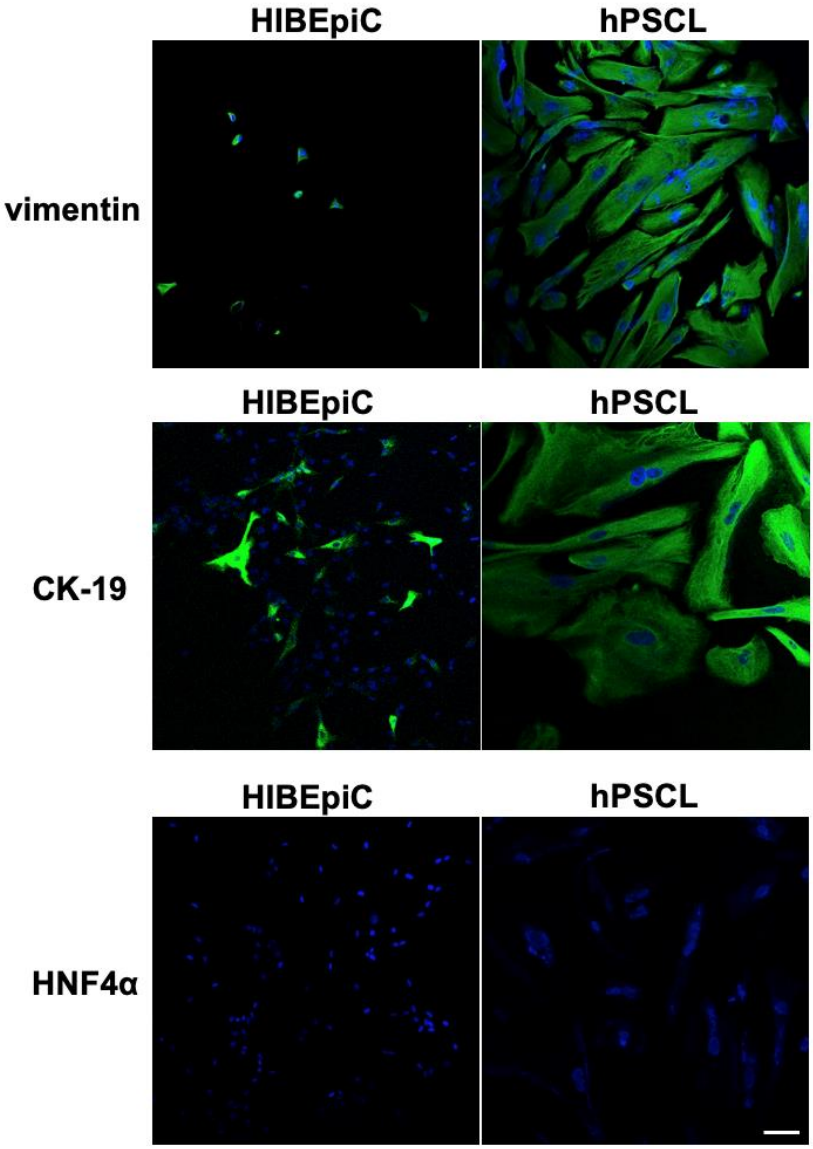

Figure 11: Expression of vimentin in hPSCL and HIBEpiCs. Immunofluorescence for vimentin, CK-19 and HNF4α (in green) in hPSCL and HIBEpiCs. Nuclei are stained with DAPI. Original magnification 20X, scale bar = 50 μm.

Loss of Vimentin Reduces Mesenchymal Phenotypes of Cholangiocytes Induced by TGF-β1 *In Vitro*

Since studies have suggested that TGF-β1 can induce EMT in cultured cholangiocytes (47, 50, 78), we treated HIBEpiCs with TGF-β1 either alone or in combination with control or vimentin CRISPR/Cas9 KO plasmid. Partial silencing of vimentin was demonstrated as approximately 50% knockdown efficiency when compared with basal and control KO groups (Figure 12a). We observed elevated expression of vimentin and reduced expression of E-cadherin in HIBEpiCs treated with TGF-β1 alone, which was significantly altered with the presence of vimentin CRISPR/Cas9 KO plasmid (Figure 12a). In addition, knockdown of vimentin suppressed TGF-β1-induced expression of fibrosis markers (Col1a1 and Fn1) and senescence markers (p16 and p21) in cultured HIBEpiCs (Figure 12b). Collectively, these data indicate that inhibition of vimentin reduces mesenchymal phenotype of cholangiocytes induced by TGF-β1 *in vitro*.

HHSteCs Treated with Cholangiocyte Supernatant Lacking Vimentin Have Decreased Fibrotic Reaction *In Vitro*

We incubated HHSteCs with cholangiocyte supernatant collected from WT, $Mdr2^{-/-}$, $Mdr2^{-/-}$ vimentin Vivo-Morpholino-treated, and $Mdr2^{-/-}$ mice treated with mismatched Vivo-Morpholino to evaluate the paracrine effect of cholangiocyte supernatant on HSC activation. Interestingly, there was increased expression of fibrosis markers (TGF-β1, Col1a1 and Fn1) and decreased expression of E-cadherin and senescence markers (p16 and p21) in HHSteCs treated with cholangiocyte supernatant from $Mdr2^{-/-}$ when compared

with supernatant from WT mice (Figure 13). Gene expression was altered in HHSteCs treated with cholangiocyte supernatant from Mdr2$^{-/-}$ mice treated with vimentin Vivo-Morpholino compared with supernatant from Mdr2$^{-/-}$ mice. No significant difference was observed in Mdr2$^{-/-}$ mice treated with mismatched Vivo-Morpholino when compared with Mdr2$^{-/-}$ mice (Figure 13).

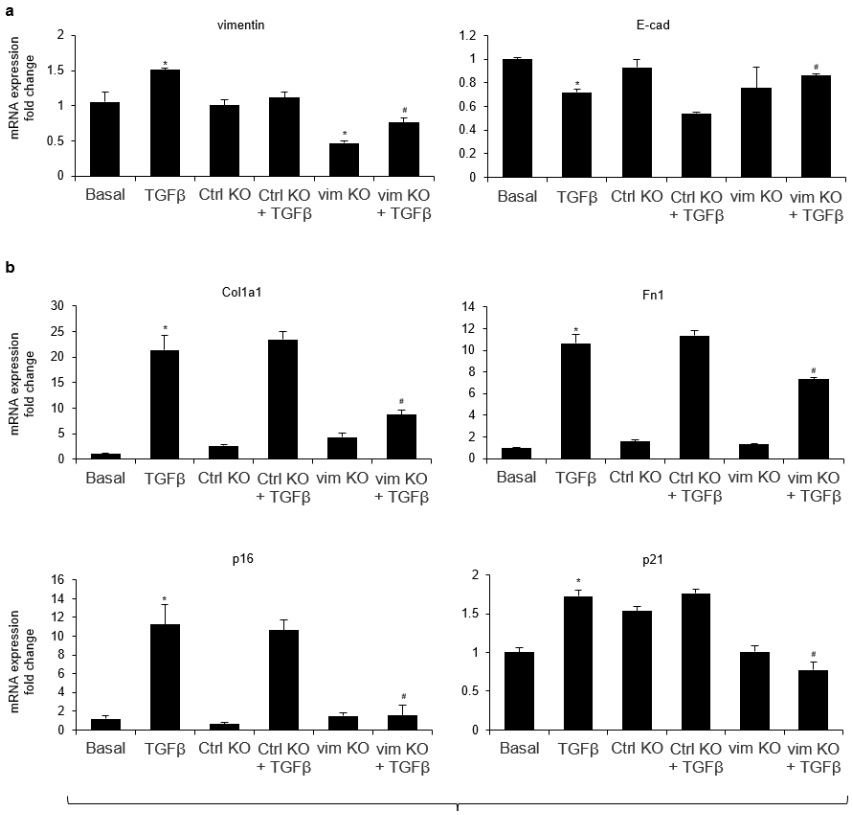

Figure 12: Loss of vimentin reduces mesenchymal phenotypes of cholangiocytes induced by TGF-β1 *in vitro*. [a-b] The mRNA expression of EMT markers (vimentin and E-cadherin), fibrotic markers (Col1a1 and Fn1) and senescence markers (p16 and p21) was evaluated by *q*PCR in basal HIBEpiCs and control or vimentin CRISPR/Cas9 KO plasmid-transfected HIBEpiCs with/without TGF-β1 stimulation. *p<0.05 versus basal HIBEpiCs; #p<0.05 versus HIBEpiCs treated with TGF-β1.

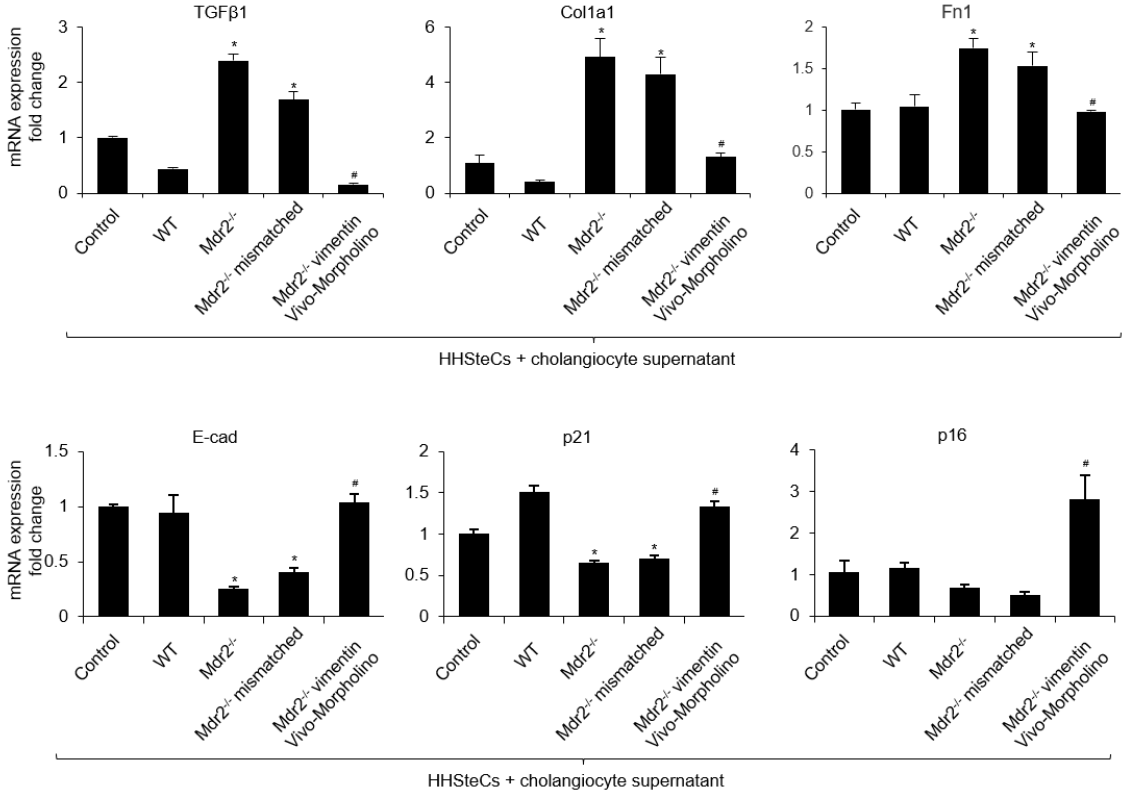

Figure 13: HHSteCs treated with cholangiocyte supernatant lacking vimentin have decreased fibrotic reaction *in vitro*. The mRNA expression of fibrotic markers (Col1a1, Fn1 and TGF-β1), senescence markers (p16 and p21) and E-cadherin was evaluated by *q*PCR in HHSteCs treated with cholangiocyte supernatant collected from WT, Mdr2$^{-/-}$, Mdr2$^{-/-}$ vimentin Vivo-Morpholino-treated and Mdr2$^{-/-}$ mice treated with mismatched Vivo-Morpholino. *p<0.05 vs. basal HHSteCs; #p<0.05 vs. HHSteCs treated with cholangiocyte supernatant from Mdr2$^{-/-}$ mice.

Validation of the $SR^{-/-}/Mdr2^{-/-}$ Mouse Model

To validate SR and Mdr2 deletion in $SR^{-/-}/Mdr2^{-/-}$ homozygous mice, genomic DNA was extracted from tail tissue and subjected to PCR genotyping analysis (Figure 14). DNA from $SR^{-/-}/Mdr2^{-/-}$ mice showed bands corresponding to the mutant alleles of both SR and Mdr2. There was enhanced immunoreactivity of SR (red arrows) in liver sections from $Mdr2^{-/-}$ compared to the corresponding WT mice (Figure 15); no immunoreactivity for SR was observed in $SR^{-/-}$ and $SR^{-/-}/Mdr2^{-/-}$ mice compared to WT mice (Figure 15, green arrowheads).

SR Depletion Ameliorates Liver Damage in $Mdr2^{-/-}$ mice

$Mdr2^{-/-}$ mice display typical features of PSC such as increased connective tissue deposition and higher inflammatory infiltration, phenotypes that were improved in $SR^{-/-}/Mdr2^{-/-}$ mice; and no significant changes were noted in $SR^{-/-}$ compared to WT mice (Figure 16). No significant changes were observed in the morphology of pancreas, heart, kidney, stomach, small and large intestine in all animal groups (Figure 16). The spleen of $Mdr2^{-/-}$ mice showed a higher presence of white pulp compared to red pulp, probably due to an increase in the inflammatory reaction (Figure 16). There was enhanced inflammatory infiltration in the pulmonary parenchyma of the lungs of $Mdr2^{-/-}$ mice that was reduced in $SR^{-/-}/Mdr2^{-/-}$ mice (Figure 16). Liver to body weight ratio increased in $Mdr2^{-/-}$ compared to the corresponding WT mice but decreased in $SR^{-/-}/Mdr2^{-/-}$ compared to $Mdr2^{-/-}$ mice (Table 4). Serum levels of SGPT, SGOT and ALP increased in $Mdr2^{-/-}$ compared to WT

mice but decreased in $SR^{-/-}/Mdr2^{-/-}$ compared to $Mdr2^{-/-}$ mice (Table 4). There were increased serum levels of TGF-β in $Mdr2^{-/-}$ compared to WT mice, levels that returned to levels similar to that of normal values in $SR^{-/-}/Mdr2^{-/-}$ mice (Table 4).

Vimentin Expression was Decreased in $SR^{-/-}/Mdr2^{-/-}$ Mice

Mesenchymal marker expression of vimentin was assessed via immunofluorescence in liver sections. Vimentin expression was increased in $Mdr2^{-/-}$ mice compared to control mice, mostly in biliary epithelium and the periductal region, as demonstrated by co-staining for CK-19 (Figure 17). However, knockout of SR reduced the expression of vimentin in $Mdr2^{-/-}$ mice.

Effects of SR Depletion on Other Mesenchymal Markers

To evaluate the effects of SR depletion on other mesenchymal markers, *q*PCR analysis of isolated cholangiocytes was performed. There was increased expression of N-cadherin, vimentin and S100A4 in $Mdr2^{-/-}$ mice compared to WT mice, changes that were reversed in $SR^{-/-}/Mdr2^{-/-}$ mice compared to $Mdr2^{-/-}$ mice (Figure 18).

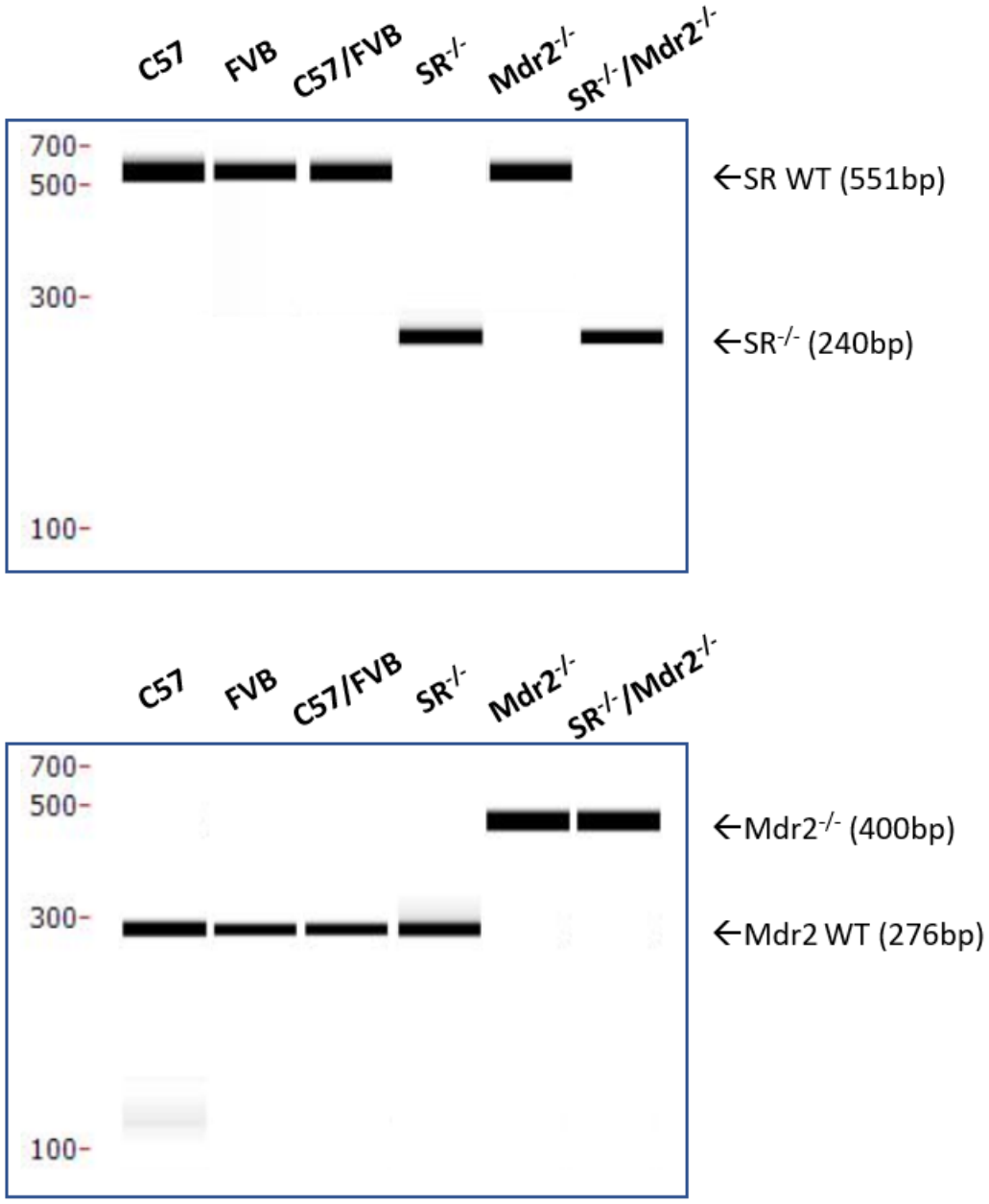

Figure 14: Genotyping for SR and Mdr2. Genomic DNA from tail tissues of all 6 animal groups were amplified by PCR for genotyping. The DNA bands corresponding to the WT and mutant alleles are marked on the right. Top, SR; Bottom, Mdr2.

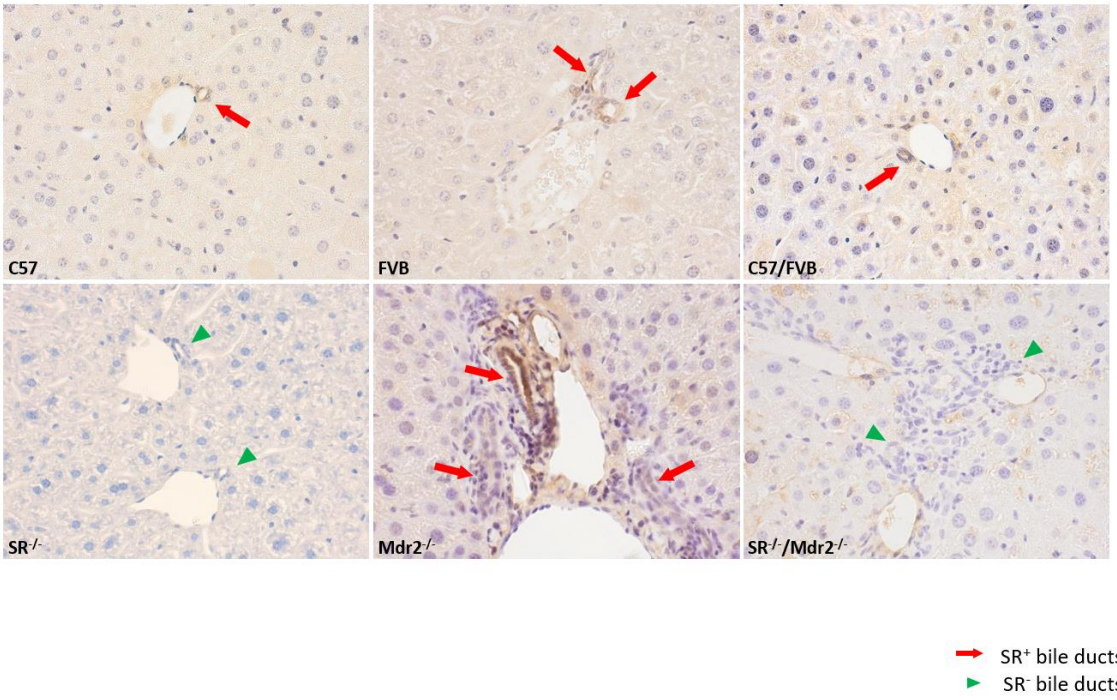

Figure 15: Expression of SR in liver sections. Immunohistochemistry for SR shows that Mdr2$^{-/-}$ mice have higher immunoreactivity for SR (red arrows depicting bile ducts) compared to WT mice. No immunoreactivity was observed for SR in SR$^{-/-}$ and SR$^{-/-}$/Mdr2$^{-/-}$ mice (green arrowheads). Original magnification 40X.

Table 4: Liver and body weight, liver/body weight ratio, serum chemistry and TGF-β1 levels in $SR^{-/-}/Mdr2^{-/-}$ mice and relevant controls.

	C57	FVB	C57/FVB	$SR^{-/-}$	$Mdr2^{-/-}$	$SR^{-/-}/Mdr2^{-/-}$
Liver weight (gm)	1.7±0.3 n=34	1.6±0.1 n=13	1.6±0.1 n=12	1.6±0.4 n=15	2.6±0.1* n=15	2.2±0.1 n=11
Body weight (gm)	26.0±0.5 n=34	30.0±0.5 n=13	31.1±1.4 n=12	32.0 ± 1.5 n=15	30.6±0.4 n=15	30.6±1.1 n=11
Liver to body weight ratio (%)	6.4±0.2 n=34	5.4±0.1 n=13	5.2±0.3 n=12	5.7±0.2 n=15	8.5±0.3* n=15	7.2±0.1# n=11
SGPT (Units/L)	326.3±32.6 n=4	131.3±16.6 n=4	124.3±11.9 n=4	321.5±68.4 n=4	1153.5±55.6* n=4	794.5±21.9# n=4
SGOT (Units/L)	485.0±53.5 n=4	431.3±25.9 n=4	570±89.8 n=4	427.5±174.3 n=4	1710.3±216.8* n=4	893.8±102.8# n=4
ALP (Units/L)	<45±5.0 n=4	<50±0.0 n=4	<56.5±6.5 n=4	<47.25±2.8 n=4	342.5±27.2* n=4	237.0±17.5# n=4
TGF-β1 levels in serum (pg/ml)	276.9±36.3 n=4	78.7±4.7 n=4	118.5±10.2 n=4	69.4±0.8 n=4	7970.7±304.8* n=4	1617.5±132.3# n=4
TGF-β1 levels in cholangiocyte supernatant (ng/ml)	4.0±0.5 n=4	0.5±0.3 n=4	1.3±0.5 n=4	24.7±1.2 n=4	764.5±30.0* n=4	216.9±10.6# n=4

*P<0.05 vs. WT mice; #P<0.05 vs. $Mdr2^{-/-}$ mice.

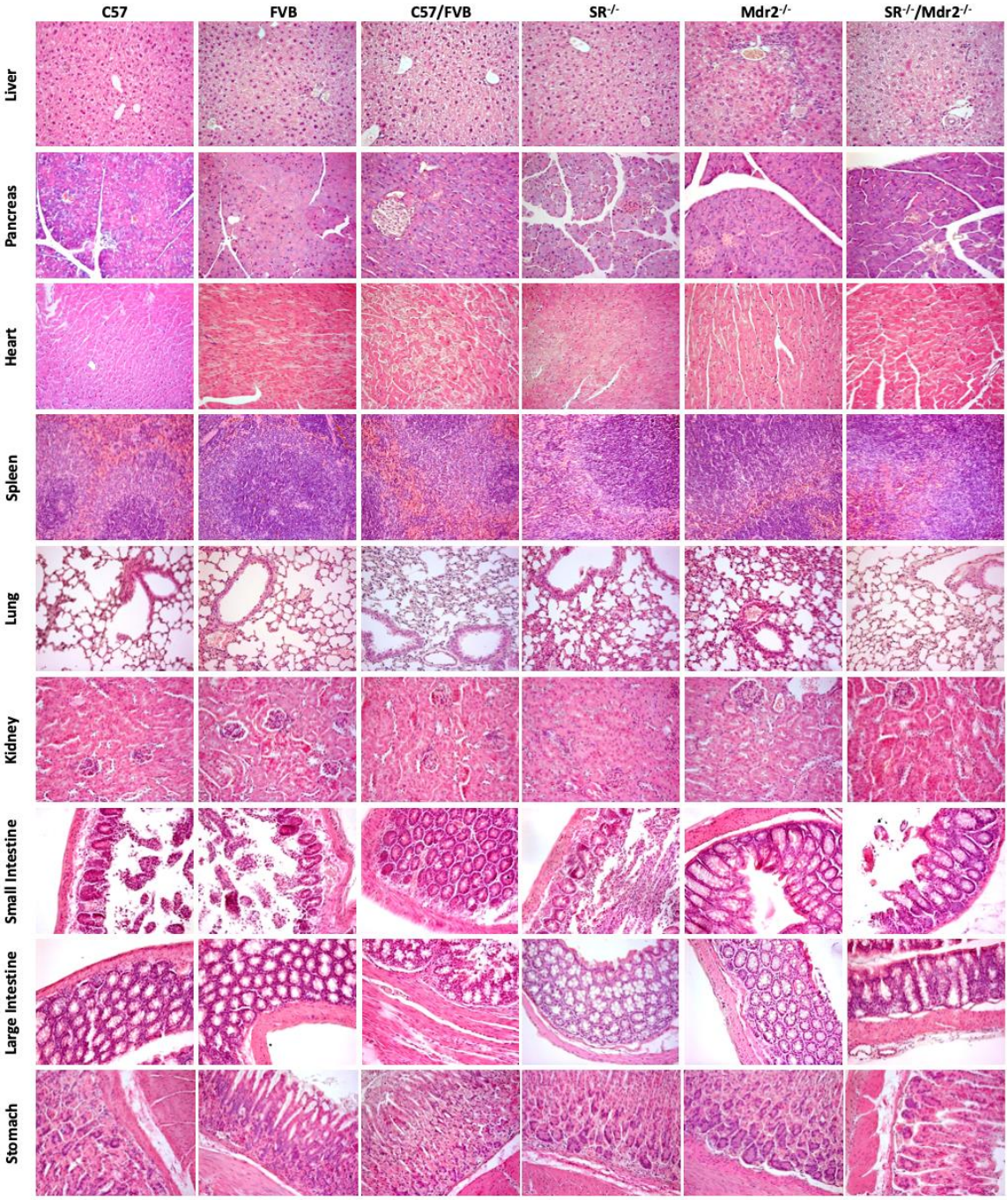

Figure 16 H&E staining in different organs. Morphology of liver, pancreas, heart, spleen, lung, kidney, stomach, small and large intestine was evaluated by H&E staining. Original magnification 20X.

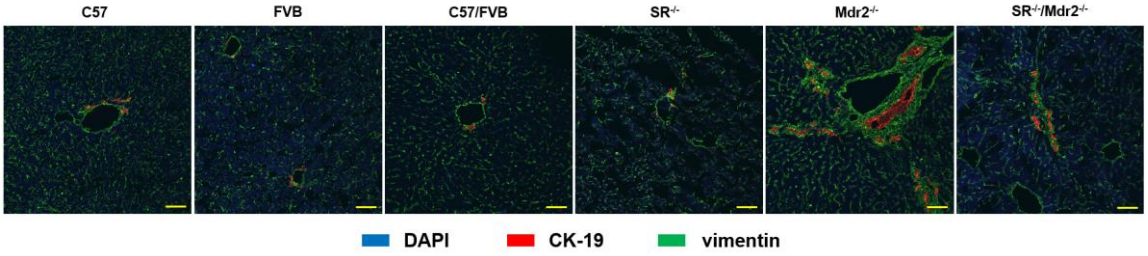

Figure 17: Vimentin expression was decreased in $SR^{-/-}/Mdr2^{-/-}$ mice. Mesenchymal marker expression of vimentin was assessed via immunofluorescence in liver sections. Vimentin expression was increased in $Mdr2^{-/-}$ mice compared to WT mice, mostly in biliary epithelium and the periductal region as indicated by co-staining for CK-19. However, knockout of SR reduced expression of vimentin. Nuclei are stained with DAPI. Original magnification 20X, scale bar = 100 μm.

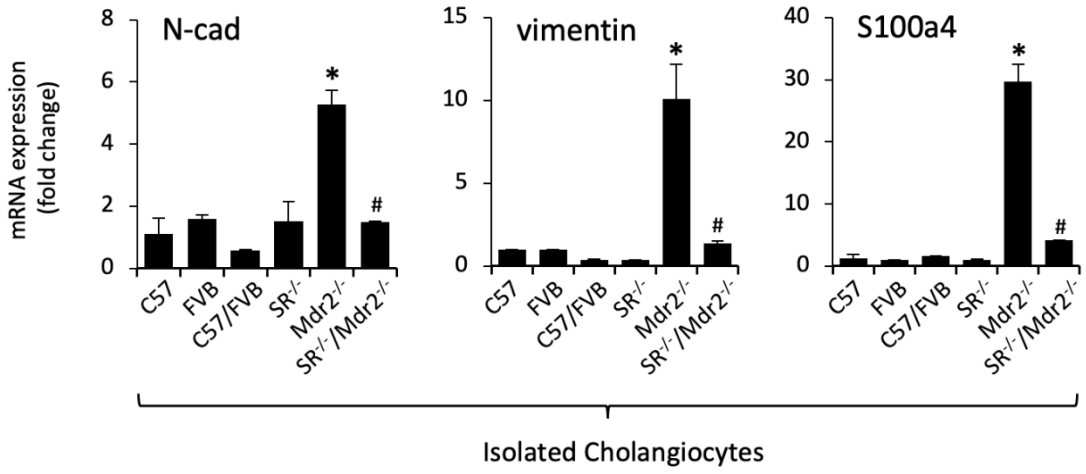

Figure 18: Effects of SR depletion on other mesenchymal markers. Evaluation of mesenchymal markers in isolated cholangiocytes by *q*PCR. There was increased expression of N-cadherin, vimentin and S100A4 in $Mdr2^{-/-}$ mice compared to WT mice, changes that were reversed in $SR^{-/-}/Mdr2^{-/-}$ mice compared to $Mdr2^{-/-}$ mice.

IBDM was Decreased in $SR^{-/-}/Mdr2^{-/-}$ Mice

In $Mdr2^{-/-}$ mice, there was increased IBDM compared to WT mice, which was reduced in $SR^{-/-}/Mdr2^{-/-}$ compared to $Mdr2^{-/-}$ mice (Figure 19a); no significant changes in IBDM were noted in $SR^{-/-}$ compared to WT mice (Figure 19a). There was increased expression of PCNA and Ki67 in cholangiocytes from $Mdr2^{-/-}$ mice, which was decreased in $SR^{-/-}/Mdr2^{-/-}$ compared to $Mdr2^{-/-}$ mice (Figure 19b, 20); no significant changes were observed in the biliary expression of PCNA and Ki67 in $SR^{-/-}$ mice compared to WT mice (Figure 19b).

Knockout of SR Decreased Liver Fibrosis in $Mdr2^{-/-}$ Mice

There was enhanced collagen deposition in liver sections from $Mdr2^{-/-}$ compared to WT mice, which was significantly decreased in $SR^{-/-}/Mdr2^{-/-}$ compared to $Mdr2^{-/-}$ mice (Figure 21a). By immunofluorescence in liver sections, there was enhanced immunoreactivity for Col1a1 (green color co-stained with CK-19, red) in $Mdr2^{-/-}$ compared to WT mice, which was reduced in $SR^{-/-}/Mdr2^{-/-}$ compared to $Mdr2^{-/-}$ mice (Figure 21b). Similarly, there was enhanced co-localization of α-SMA (red) and desmin (green) in HSCs from $Mdr2^{-/-}$ compared to WT mice, immunoreactivity that was decreased in $SR^{-/-}/Mdr2^{-/-}$ compared to $Mdr2^{-/-}$ mice (Figure 21c). In addition, there was enhanced expression of Col1a1 and FN-1 in isolated cholangiocytes and HSCs from $Mdr2^{-/-}$ mice compared to the corresponding WT mice, increase that was significantly reduced in $SR^{-/-}/Mdr2^{-/-}$ mice compared to $Mdr2^{-/-}$ mice (Figure 20, 21d).

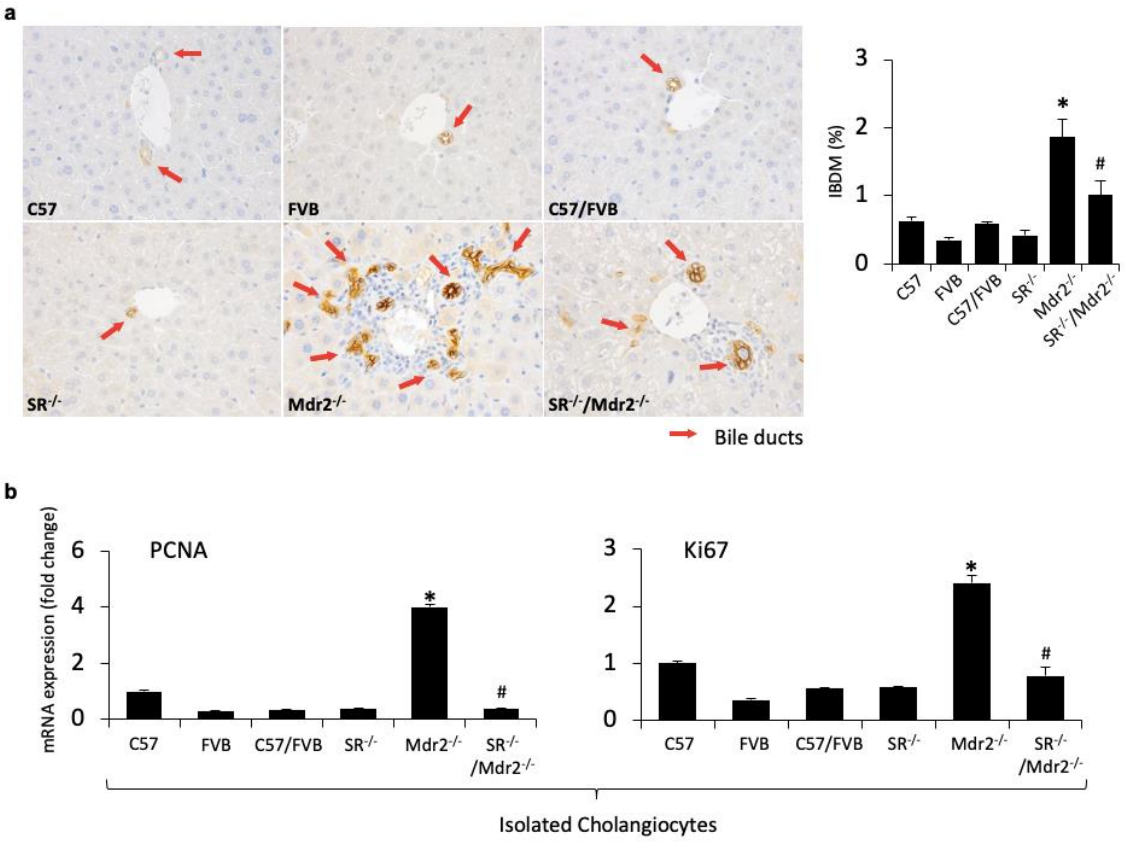

Figure 19: Measurement of ductular reaction. [a] There was increased IBDM (red arrows) in $Mdr2^{-/-}$ mice compared to WT mice, which was reduced in $SR^{-/-}/Mdr2^{-/-}$ mice compared to $Mdr2^{-/-}$ mice; no significant changes in IBDM were noted in $SR^{-/-}$ compared to WT mice. Original magnification 40X. [b] There was increased mRNA expression of PCNA and Ki67 in cholangiocytes from $Mdr2^{-/-}$ mice, which was decreased in $SR^{-/-}/Mdr2^{-/-}$ compared to $Mdr2^{-/-}$ mice. *$p<0.05$ versus FVB mice; #$p<0.05$ versus $Mdr2^{-/-}$ mice.

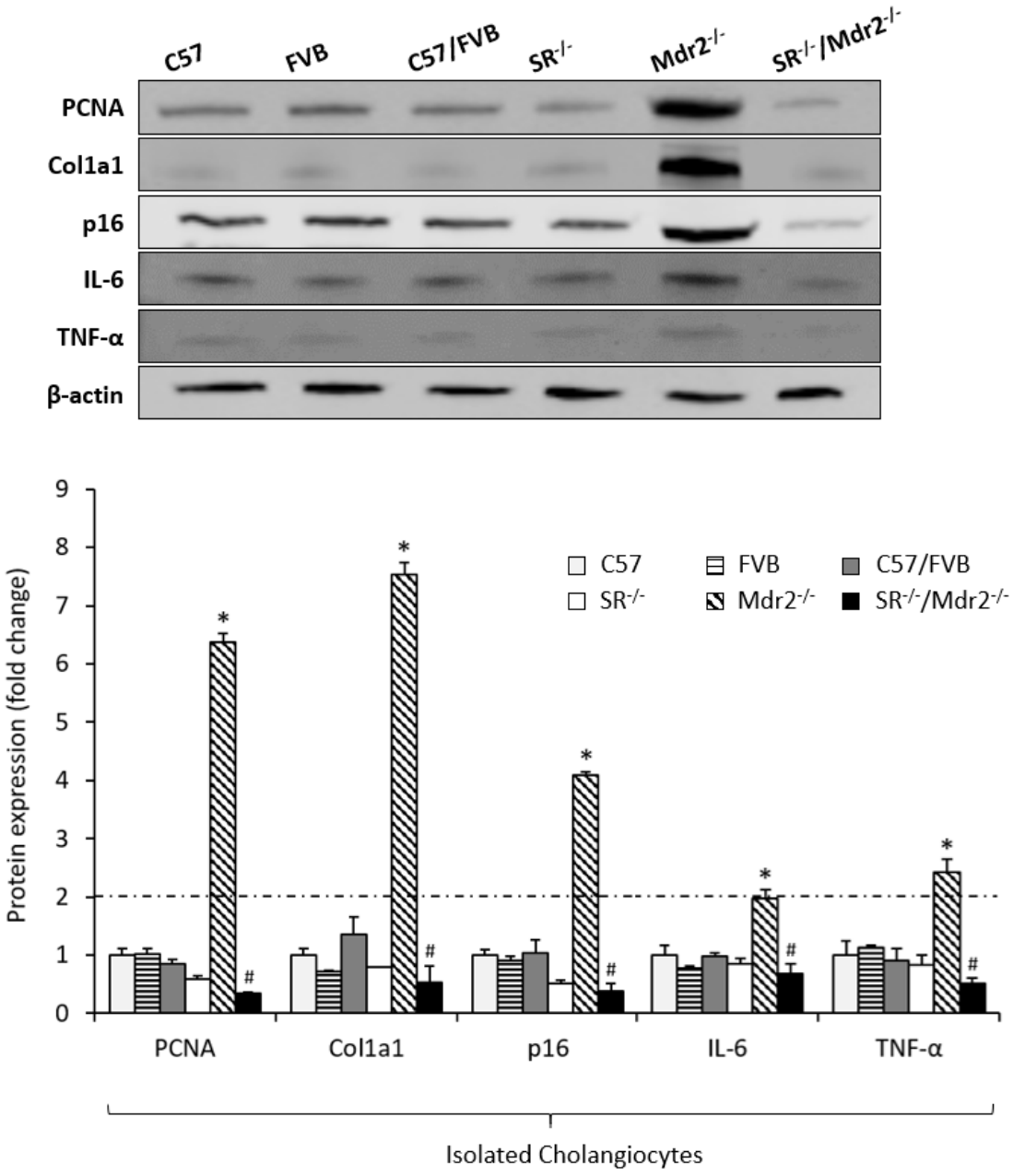

Figure 20: Western blot data for isolated cholangiocytes. Representative western blot images (of n=3 western blots for each protein) for the expression of PCNA, Col1a1, p16, IL-6 and TNF-α in isolated cholangiocytes. Protein expression levels were normalized to β-actin. Data are presented as mean ± SEM. *$p<0.05$ vs. FVB mice; #$p<0.05$ vs. $Mdr2^{-/-}$ mice.

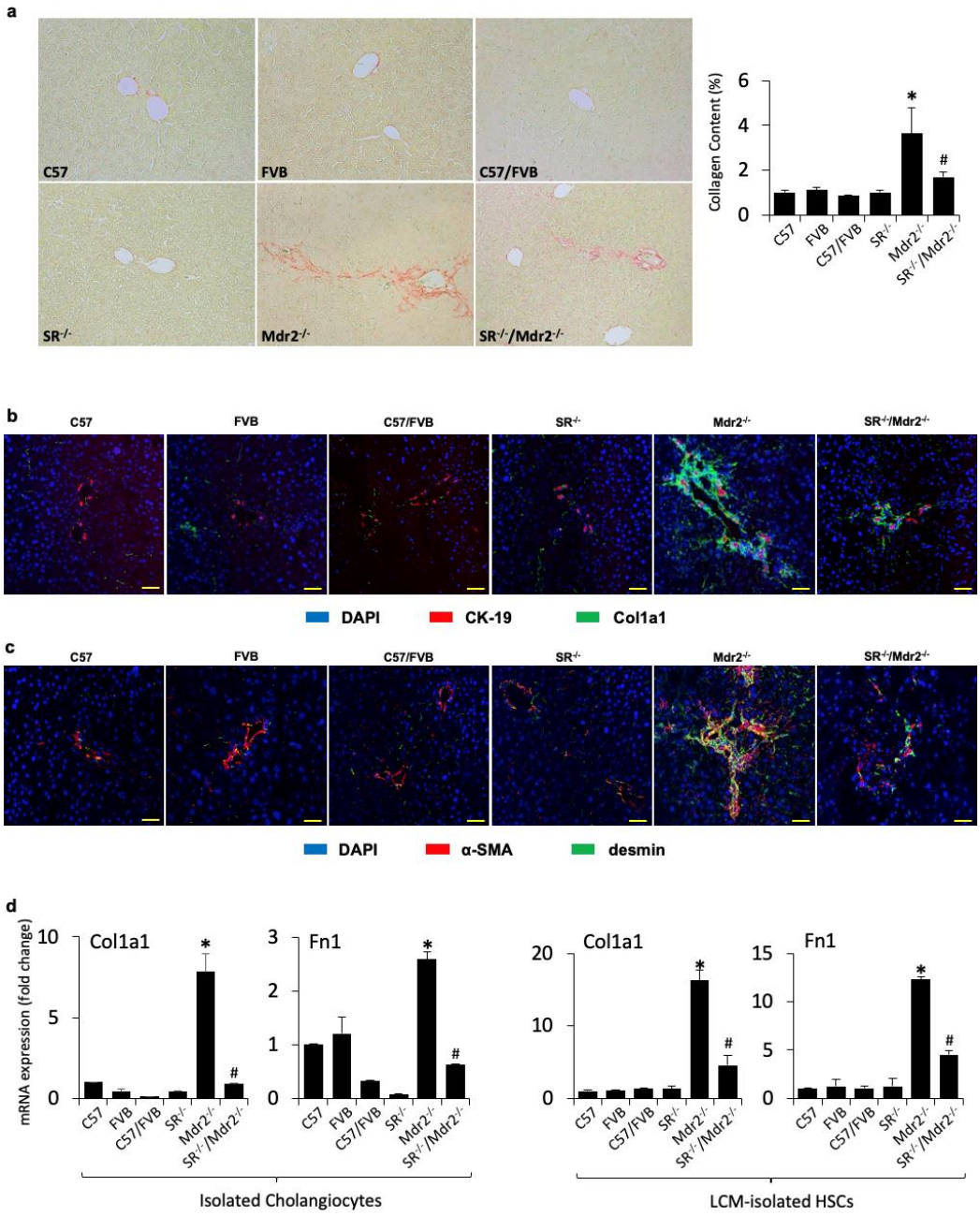

Figure 21: Knockout of SR decreased liver fibrosis in Mdr2$^{-/-}$ mice. [a] Measurement of collagen deposition in liver sections. Orig. magnification 20X. [b-c] Immunofluorescence for Col1a1 (green color, costained for CK-19 in red) and α-SMA (green color, costained for desmin in red) in liver sections. Scale bar = 100 μm. [d] *q*PCR for fibrotic markers in isolated cholangiocytes and HSCs. Data are mean ± SEM. *p<0.05 vs. FVB mice; #p<0.05 vs. Mdr2$^{-/-}$ mice.

Biliary Senescence and Activation of HSCs were Decreased in $SR^{-/-}/Mdr2^{-/-}$ Mice

IPA was performed to ascertain the cellular context of the differentially expressed signaling mechanisms related to the Sct/SR axis-mediated liver injury. IPA demonstrated that the cellular senescence pathway was likely linked to altered signaling through p16 and CCL2-related pathological mechanisms (related by the Sct/SR axis) (Fig. 22). To evaluate the underlying mechanisms by which the modulation of SR expression regulates liver fibrosis, we evaluated the effect of SR knock-out on cellular senescence in liver sections, isolated cholangiocytes and HSCs. By SA-β-gal staining in liver sections there was enhanced biliary senescence from $Mdr2^{-/-}$ compared to WT mice, which was significantly decreased in $SR^{-/-}/Mdr2^{-/-}$ when compared to $Mdr2^{-/-}$ mice (Figure 23a). By immunofluorescence in liver sections from $Mdr2^{-/-}$ mice, there was enhanced immunoreactivity for p16 (co-stained for CK-19) in cholangiocytes compared to WT mice, immunoreactivity that was reduced in $SR^{-/-}/Mdr2^{-/-}$ compared to $Mdr2^{-/-}$ mice (Figure 23b). There was enhanced expression of p16 and CCL2 in cholangiocytes from $Mdr2^{-/-}$ mice compared to WT mice, which decreased in $SR^{-/-}/Mdr2^{-/-}$ compared to $Mdr2^{-/-}$ mice (Figure 20, 23c). Conversely, the expression of p16 and CCL2 was significantly decreased in HSCs from $Mdr2^{-/-}$ compared to WT mice, changes that returned to values similar to those of the normal WT group in $SR^{-/-}/Mdr2^{-/-}$ mice (Figure 23c).

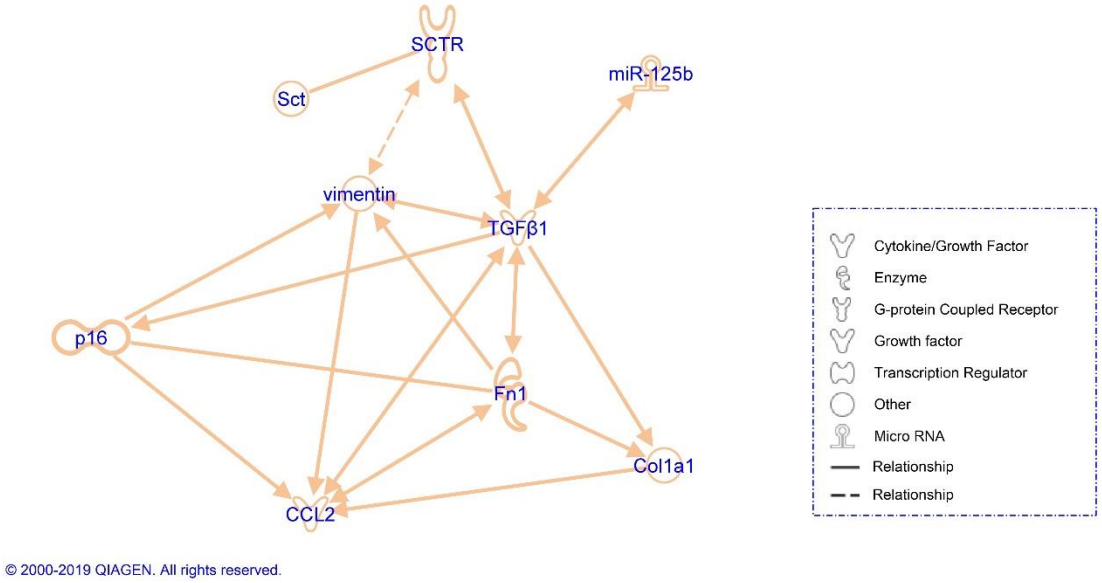

Figure 22: IPA signaling. IPA software identifies downstream target genes of fibrosis and senescence that are regulated by the Sct/SR axis.

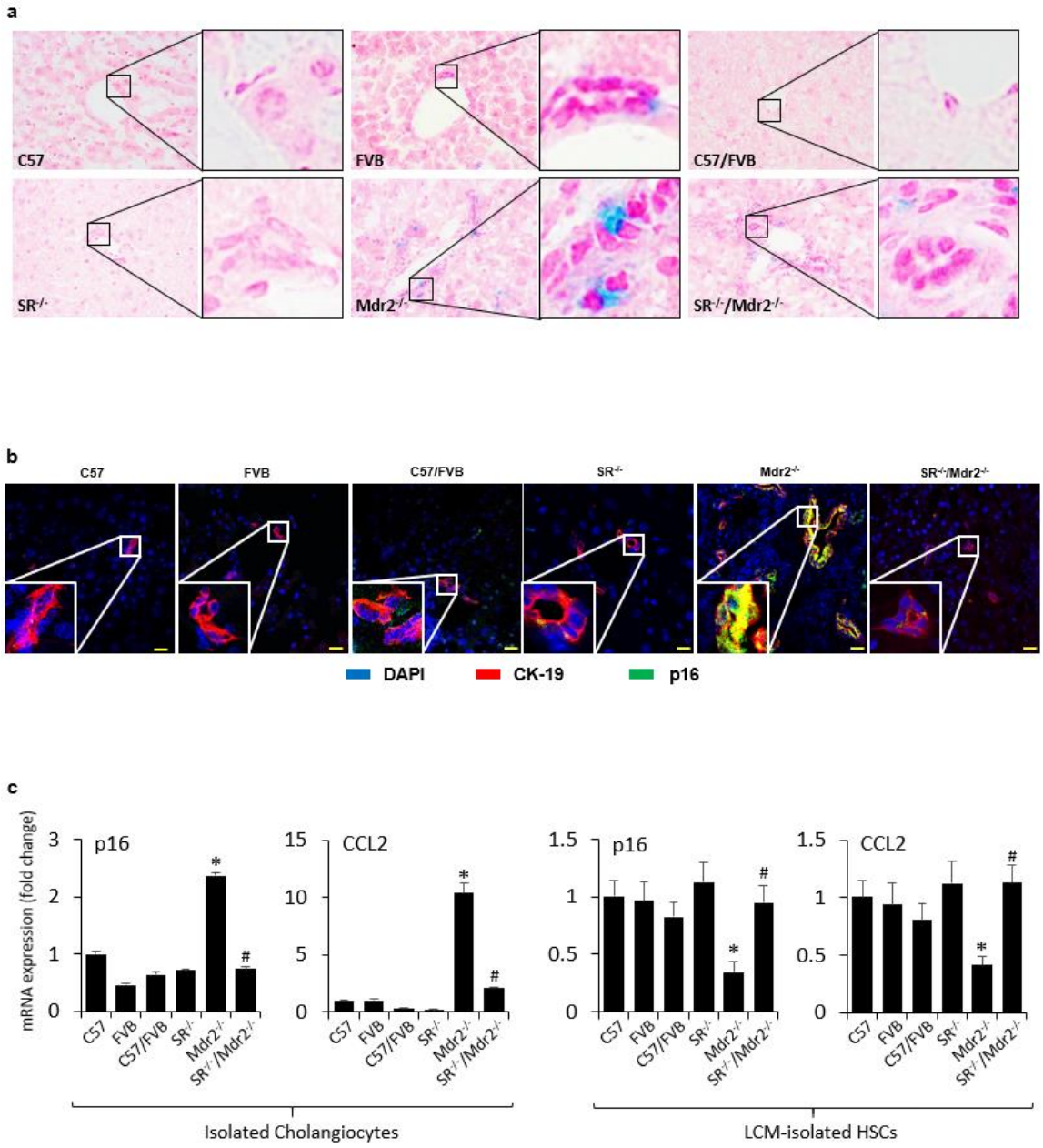

Figure 23: Biliary senescence and activation of HSCs were decreased in SR$^{-/-}$/Mdr2$^{-/-}$ mice. [a] Measurement of cellular senescence in liver sections by SA-β-gal staining in liver sections (original magnification 40X) [b] Immunofluorescence for p16 (green, co-stained for CK-19, red) in liver sections, nuclei are stained with DAPI. Scale bar = 20 μm. [c] Results of *q*PCR for senescence markers in isolated cholangiocytes and HSCs. Data are mean ± SEM. *p<0.05 vs. FVB mice; #p<0.05 vs. Mdr2$^{-/-}$ mice.

Loss of SR Reduced Secretin Levels and the Expression of MicroRNA 125b in Mdr2$^{-/-}$ Mice

Secretin levels in cholangiocyte supernatants were increased in Mdr2$^{-/-}$ mice compared to WT mice, and decreased in SR$^{-/-}$/Mdr2$^{-/-}$ compared to Mdr2$^{-/-}$ mice (Figure 24a). The expression of microRNA 125b was decreased in cholangiocytes from Mdr2$^{-/-}$ compared to WT mice, expression that returned to values similar to that of the normal WT group in SR$^{-/-}$/Mdr2$^{-/-}$ mice (Figure 24b).

Hepatic Inflammation was Decreased in SR$^{-/-}$/Mdr2$^{-/-}$ Mice

We observed enhanced levels of IL-6 and TNF-α in cholangiocytes from Mdr2$^{-/-}$ mice compared to WT mice but decreased levels in cholangiocytes from SR$^{-/-}$/Mdr2$^{-/-}$ compared to Mdr2$^{-/-}$ mice (Figure 25a). Mouse cytokine array showed increased inflammatory cytokine expression in cholangiocyte supernatants from Mdr2$^{-/-}$ mice compared to WT mice, which decreased in SR$^{-/-}$/Mdr2$^{-/-}$ compared to Mdr2$^{-/-}$ mice, suggesting SR regulates the inflammatory response in cholangiocytes (Figure 25b).

TGF-β1 Levels were Decreased in SR$^{-/-}$/Mdr2$^{-/-}$ Mice

There were enhanced levels of TGF-β1 in cholangiocyte supernatants from Mdr2$^{-/-}$ mice, levels that returned to values similar to that of the WT group in cholangiocyte supernatants from SR$^{-/-}$/Mdr2$^{-/-}$ mice (Table 4).

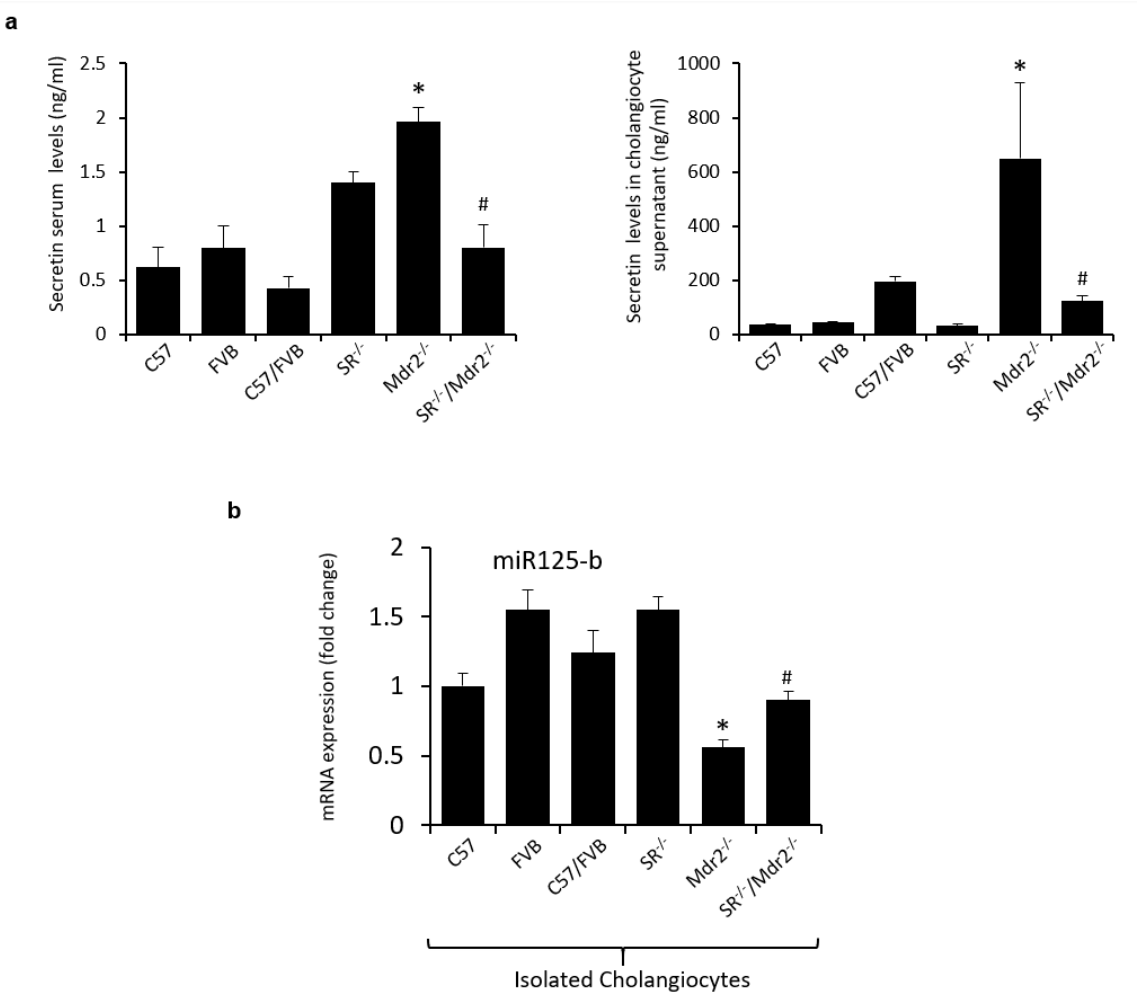

Figure 24: Loss of SR reduced secretin and miR-125b levels in Mdr2$^{-/-}$ mice. [a] Secretin levels were measured in collected serum and cholangiocyte supernatants with an ELISA kit. Data are mean ± SEM. *p<0.05 vs. FVB mice; #p<0.05 vs. Mdr2$^{-/-}$ mice. [b] Results of *q*PCR for miR-125b in isolated cholangiocytes. Data were normalized to a housekeeping gene, U6. Data are mean ± SEM. *p<0.05 vs. FVB mice; #p<0.05 vs. Mdr2$^{-/-}$ mice.

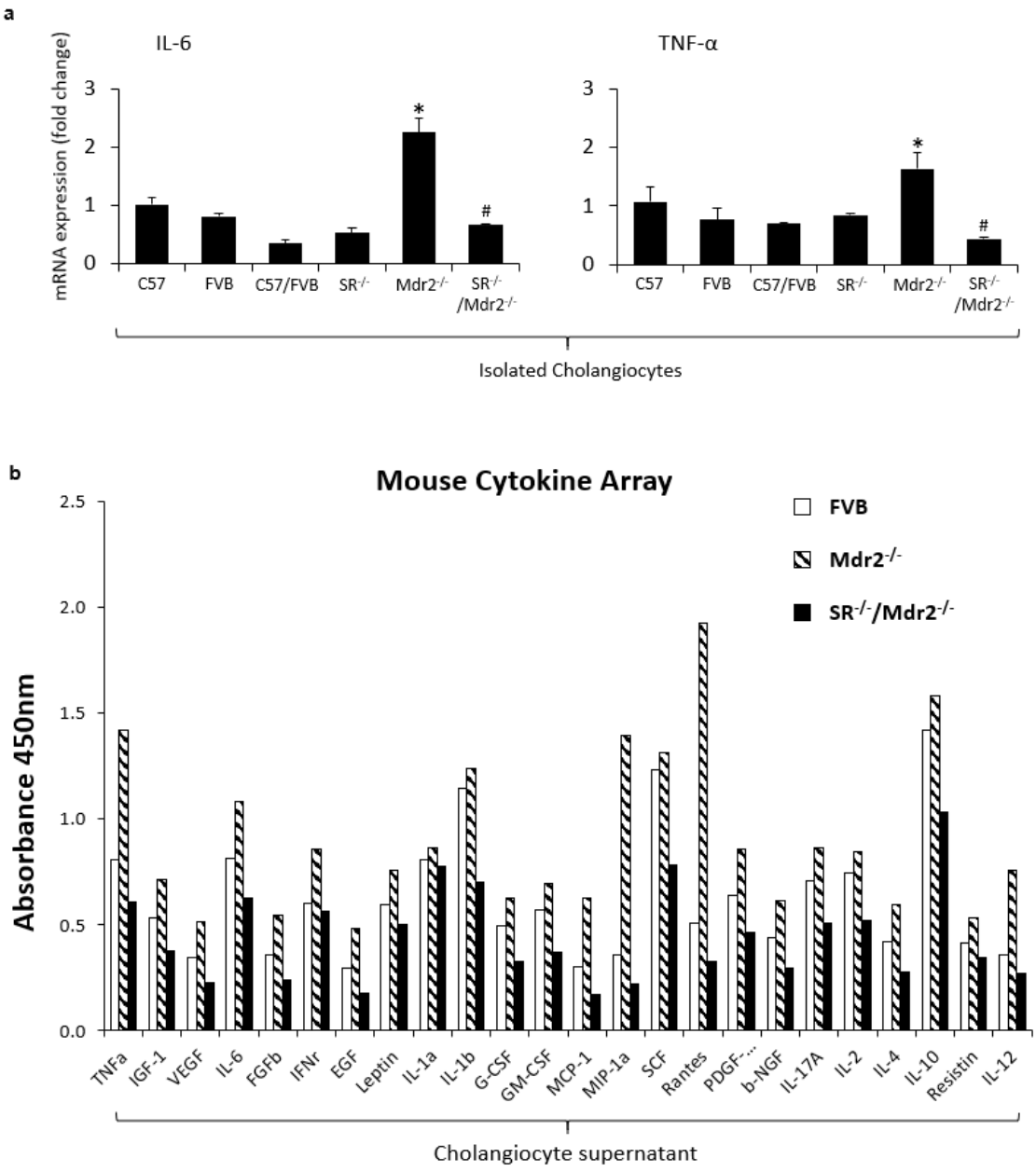

Figure 25: Hepatic inflammation was decreased in SR$^{-/-}$/Mdr2$^{-/-}$ mice. [a] Results of *q*PCR for inflammatory markers (IL-6 and TNF-α) in isolated cholangiocytes. Data are mean ± SEM. *p<0.05 vs. FVB mice; #p<0.05 vs. Mdr2$^{-/-}$ mice. [b] Mouse cytokine array was performed using cholangiocyte supernatants.

In Vitro Paracrine Effect of Cholangiocyte Supernatant on the Expression of Senescent and Fibrosis Genes in HHSteCs

There was increased gene expression of fibrosis markers but decreased senescence gene expression in HHSteCs treated with cholangiocyte supernatants from $Mdr2^{-/-}$ mice compared to HHSteCs treated with supernatant from WT mice; the gene expression of fibrosis markers matched normal levels when HHSteCs were treated with cholangiocyte supernatant from $SR^{-/-}/Mdr2^{-/-}$ mice (Figure 26a). These effects were also reversed when HHSteCs were preincubated with LY2109761 (a TGF-β1 receptor antagonist) before treatment with the cholangiocyte supernatants from $Mdr2^{-/-}$ mice (Figure 26b).

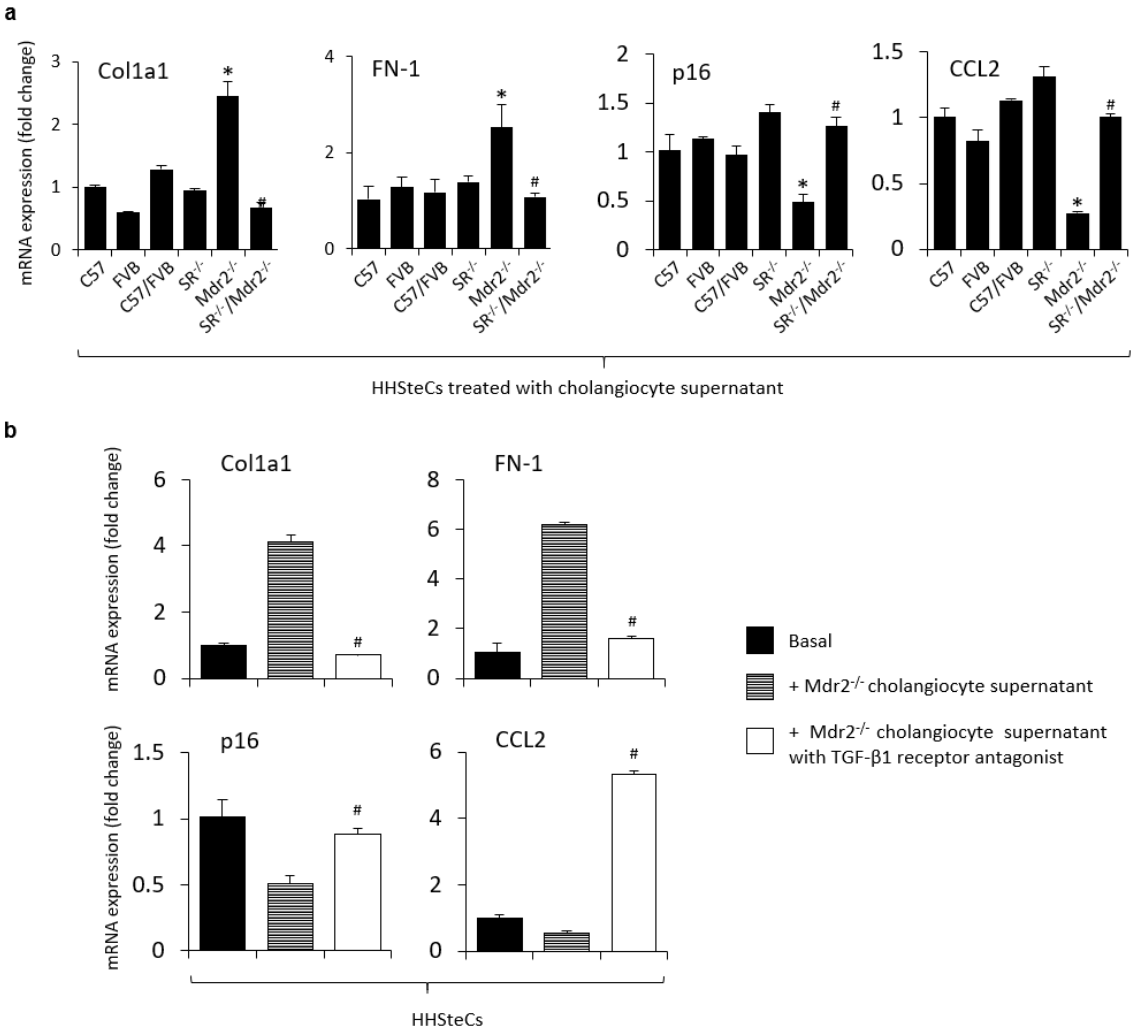

Figure 26: TGF-β1 receptor antagonist reversed the fibrotic reaction in HHSteCs. [a] Results of *q*PCR for fibrosis and senescence markers in HHSteCs treated with cholangiocyte supernatants. Data are mean ± SEM. *p<0.05 vs. HHSteCs treated with FVB mice derived cholangiocyte supernatants. #p<0.05 vs. HHSteCs treated with cholangiocyte supernatants from Mdr2$^{-/-}$ mice. [b] Results of *q*PCR for fibrosis and senescence markers in HHSteCs treated with cholangiocyte supernatants from Mdr2$^{-/-}$ mice with or without the TGF-β1 receptor antagonist, LY2109761. #p<0.05 vs. HHSteCs treated with cholangiocyte supernatants from Mdr2$^{-/-}$ mice.

CHAPTER IV

CONCLUSION

The main findings of the present study indicate that there was: (1) enhanced expression of mesenchymal phenotypes in cholangiocytes of $Mdr2^{-/-}$ mice, which was reduced by treatment with vimentin Vivo-Morpholino as well as genetical depletion of SR; and (2) liver damage, ductular reaction, biliary senescence and liver fibrosis that were concomitantly decreased in $Mdr2^{-/-}$ vimentin Vivo-Morpholino-treated mice as well as $SR^{-/-}/Mdr2^{-/-}$ mice. We also demonstrated that: (i) overexpression of vimentin and other mesenchymal markers were observed in PSC patients and hPSCL cells compared to healthy controls and HIBEpiCs (normal cholangiocyte lines), respectively; (ii) *in vitro* silencing of vimentin reduced TGF-β1-induced mesenchymal phenotypes of HIBEpiCs; and (iii) HHSteCs treated with cholangiocyte supernatants with reduced levels of vimentin and TGF-β1 displayed decreased fibrotic reaction.

EMT is a phenomenon that has been identified in several types of chronic fibrotic disorders, where epithelial cells acquire mesenchymal features, thereby contributing to the fibrogenic process (79, 80). EMT has also been observed in embryonic development and tumor progression (81, 82). The key steps of EMT include loss of epithelial cell-cell adhesion and degradation of junctional proteins, including E-cadherin; and upregulation of cytoskeletal proteins belonging to the mesenchymal lineage, including vimentin, S100a4 and, eventually, α-SMA (48). Additional changes during EMT include the generation of fibroblasts associated with accumulation of extracellular matrix and

increased matrix metalloproteinases (MMPs), particularly MMP2 and MMP9 during liver fibrosis (47, 83). In the current study, we found that there were enhanced mesenchymal phenotypes of cholangiocytes in $Mdr2^{-/-}$ compared to WT mice, which may contribute to the population of portal fibroblasts (48, 49, 83). Although our data support the existence of cholangiocytes with a mesenchymal phenotype, it is contradictory to the findings by Chu et al., who used Alfp-Cre x Rosa26-YFP mice to achieve lineage tracing for all epithelial cells of the liver (hepatocytes, cholangiocytes, and their bipotential progenitors) with yellow fluorescent protein (YFP) (50). They found no evidence of YFP co-localization with the mesenchymal markers S100a4, vimentin or α-SMA in mouse models of liver fibrosis, including BDL and CCl_4 treatment; however, several factors may explain this discrepancy. First, the studies were conducted with different animal models from the ones in our study. Although all three models are widely used in the experimental liver fibrosis setting, $Mdr2^{-/-}$ mice have been recognized to share several important morphologic and pathogenetic characteristics with human PSC patients (40, 84-86). Second, different experimental approaches were utilized to evaluate mesenchymal traits. We realize that immunostaining itself may cause many nonspecific signals and some mesenchymal markers may not be cell-type specific, which limits the specificity of this technique. However, lineage tracing studies using the Cre-LoxP system also has some pitfalls. The efficiency of Cre-mediated recombination is not 100%. It is theoretically possible that mesenchymal transition might have occurred in the non-labeled cells. Furthermore, we demonstrated in the current study that overexpression of vimentin and decreased CK-19 staining intensity were observed in PSC patients compared with healthy controls.

Interestingly, E-cadherin protein expression was not decreased in PSC patients, which might be due to the abundant E-cadherin expressed in hepatocytes. Although loss of E-cadherin has been recognized as a hallmark of EMT, the observation of maintained E-cadherin expression in cholangiocytes has also been demonstrated by Yasunori et al. (80). With regard to hepatocellular carcinoma (HCC), E-cadherin expression is commonly variable and is elevated in 40% of HCC cases, suggesting its paradoxical roles in liver diseases (87-89). Another study has demonstrated that cholangiocytes within sites of ductular reaction from patients with PSC, PBC and alcoholic cirrhosis showed significant induction of S100a4, MMP2 and vimentin, suggesting that the development of portal tract fibrosis is associated with local induction of an EMT process (47). However, no co-localization of CK-19 and α-SMA were observed in human liver sections, which we believe is because only mature myofibroblasts express α-SMA and they may have already lost the expression of CK-19 after migration.

The molecular mechanisms that regulate changes in EMT include paracrine and autocrine factors (cytokines, proinflammatory mediators, and growth factors), and several signaling pathways (TGF-β, Hedgehog and Wnt/β-catenin) (83). Among these signaling pathways, the TGF-β1 pathway is critical to the progression of fibrosis and is the major inducer of EMT. TGF-β1 binds to the functional complex of the TGF-β receptor family at the cell surface, which leads to the phosphorylation of Smad2/3 (8, 90, 91). Studies using cultured cholangiocytes have shown that TGF-β1 treatment evoked a decrease in the expression of epithelial markers and an increase in the expression of vimentin and other mesenchymal markers (80, 92, 93). In the current study, we found that the effects of

inhibiting vimentin in Mdr2$^{-/-}$ mice on mesenchymal phenotypes of cholangiocytes and liver fibrosis were associated with decreased levels of TGF-β1. Furthermore, cellular senescence and its associated secretion of SASP factors (e.g., TGF-β1, p16 and SA-β-gal) have been considered as key hallmarks of cholangiopathies, including PSC and PBC, and contribute to enhanced liver fibrosis (11, 70). We have previously shown that TGF-β1 increases biliary senescence by an autocrine loop, which in turn leads to the paracrine activation of HSCs by cholangiocytes (11). In addition, as we have shown that SASP factors secreted by cholangiocytes attracted macrophages to the periductular area during liver damage. The increased number of macrophages also secrete inflammatory cytokines and other factors, which may alter cholangiocyte phenotype and secretory function in a paracrine manner.

Changes in ductular reaction in response to cholestatic liver injury are modulated by a number of neuroendocrine/gastrointestinal factors such as melatonin, gastrin, histamine, sex hormones and Sct (5, 94, 95). Among these neuroendocrine factors, Sct (which exerts its effects by selective interaction with basolateral SR expressed only by cholangiocytes) plays a key role in the autocrine modulation of biliary damage/proliferation/homeostasis in addition to the paracrine regulation of liver inflammation and fibrosis (8, 57, 58). For example, we have previously shown that: (i) Sct increases ductular reaction by both autocrine and paracrine pathways through upregulation of cAMP-dependent protein kinase A signaling as well as microRNA 125b-dependent VEGF-A expression (58, 94, 96); and (ii) knockout of the Sct/SR axis reduces biliary hyperplasia as well as liver fibrosis by a paracrine mechanism involving a

microRNA 125b-dependent decrease of biliary TGF-β1 secretion (8, 58). IPA indicated that the Sct/SR axis is a major upstream regulator of the pathway networks under our experimental conditions, perhaps suggesting a central role of Sct in regulating biliary senescence and fibrosis. However, our previous studies have limitations because we did not evaluate the potential role of the Sct/SR axis on the modulation of cellular senescence that may affect both the senescence of cholangiocytes (by an autocrine loop) as well as the senescence of HSCs by a paracrine mechanism associated with the release of SASP factors (e.g., TGF-β1, IL-6, CCL2, p16/21, SA-β-gal, PAI-1 and substance P) (34, 37, 70, 97, 98) that play key roles in the activation of HSCs and liver fibrosis (10, 34). Supporting this finding, a recent *in vitro* study in the human cholangiocyte line, MMNK-1, identified by microarray analysis differentially regulated genes in response to lysophosphatidylcholine, which included IL-6, TGF-β1 and PAI-1 (98). Parallel to this line of research, we have not only demonstrated that TGF-β1 induces the activation of HSCs through decreased cellular senescence by a paracrine mechanism, but also provided novel evidence that TGF-β1 increases biliary senescence by an autocrine loop, thus further increasing the paracrine activation of HSCs by cholangiocytes. Moreover, supporting the key role of TGF-β1 in modulating biliary homeostasis and liver fibrosis, $Mdr2^{-/-}$ mice treated with the SR antagonist (Sec 5-27) displayed reduced biliary mass and HSC activation, which correlates with decreased TGF-β1 expression (8). The observation that attenuated liver fibrosis is associated with decreased senescence of cholangiocytes (associated with reduced Sct-dependent TGF-β1 expression/secretion) is consistent with the finding by Moncsek et al. who demonstrated that senescent cholangiocytes promote

the development of liver fibrosis by secretion of Bcl-XL, which is a key survival factor for several senescent cell types (10). Inhibition of Bcl-XL in $Mdr2^{-/-}$ mice depletes senescent cholangiocytes and reduces liver fibrosis.

However, one of the unsolved questions of this study is the mechanism by which the Sct/SR axis regulates the differential changes of senescence in cholangiocytes and HSCs. We postulate that this difference may be explained in terms of the heterogeneity of the biliary epithelium, as the Sct/SR axis may target different sized cholangiocytes that could respond differentially to liver injury (99). We speculate that a subset of large cholangiocytes may lose the ability to proliferate and undergo cellular senescence and subsequently interact with nearby undamaged small and large cholangiocytes inducing damage/senescence of these cells. However, additional studies are required to isolate and characterize these different subsets of cholangiocytes in order to pinpoint the specific subpopulations of cholangiocytes undergoing senescence.

In conclusion, we have identified that vimentin Morpholino treatment as well as genetically depleting SR in $Mdr2^{-/-}$ mice reduces the mesenchymal phenotype of cholangiocytes, ductular reaction, biliary senescence and liver fibrosis, and the pro-fibrotic activation of HSCs by a paracrine mechanism. Inhibition of vimentin expression may be a key therapeutic strategy in the treatment of cholangiopathies, including PSC.

REFERENCES

1. Kanno N, LeSage G, Glaser S, Alpini G. Regulation of cholangiocyte bicarbonate secretion. American journal of physiology. Gastrointestinal and liver physiology 2001;281:G612-G625.

2. Tabibian JH, Masyuk AI, Masyuk TV, O'Hara SP, LaRusso NF. Physiology of cholangiocytes. Comprehensive Physiology 2013;3:541-565.

3. Alpini G, Roberts S, Kuntz SM, Ueno Y, Gubba S, Podila PV, LeSage G, et al. Morphological, molecular, and functional heterogeneity of cholangiocytes from normal rat liver. Gastroenterology 1996;110:1636-1643.

4. Glaser SS, Gaudio E, Rao A, Pierce LM, Onori P, Franchitto A, Francis HL, et al. Morphological and functional heterogeneity of the mouse intrahepatic biliary epithelium. Laboratory investigation; a journal of technical methods and pathology 2009;89:456-469.

5. Hall C, Sato K, Wu N, Zhou T, Kyritsi K, Meng F, Glaser S, et al. Regulators of Cholangiocyte Proliferation. Gene expression 2017;17:155-171.

6. Sato K, Meng F, Giang T, Glaser S, Alpini G. Mechanisms of cholangiocyte responses to injury. Biochimica et biophysica acta. Molecular basis of disease 2018;1864:1262-1269.

7. Banales JM, Huebert RC, Karlsen T, Strazzabosco M, LaRusso NF, Gores GJ. Cholangiocyte pathobiology. Nature reviews. Gastroenterology & hepatology 2019;16:269-281.

8. Wu N, Meng F, Invernizzi P, Bernuzzi F, Venter J, Standeford H, Onori P, et al. The secretin/secretin receptor axis modulates liver fibrosis through changes in transforming growth factor-β1 biliary secretion in mice. Hepatology (Baltimore, Md.) 2016;64:865-879.

9. Zhou T, Kyritsi K, Wu N, Francis H, Yang Z, Chen L, O'Brien A, et al. Knockdown of vimentin reduces mesenchymal phenotype of cholangiocytes in the Mdr2(-/-) mouse model of primary sclerosing cholangitis (PSC). EBioMedicine 2019;48:130-142.

10. Moncsek A, Al-Suraih MS, Trussoni CE, O'Hara SP, Splinter PL, Zuber C, Patsenker E, et al. Targeting senescent cholangiocytes and activated fibroblasts with B-cell lymphoma-extra large inhibitors ameliorates fibrosis in multidrug resistance 2 gene knockout (Mdr2(-/-)) mice. Hepatology (Baltimore, Md.) 2018;67:247-259.

11. Zhou T, Wu N, Meng F, Venter J, Giang TK, Francis H, Kyritsi K, et al. Knockout of secretin receptor reduces biliary damage and liver fibrosis in Mdr2(-/-) mice by diminishing senescence of cholangiocytes. Laboratory investigation; a journal of technical methods and pathology 2018;98:1449-1464.

12. Marchioni Beery RM, Vaziri H, Forouhar F. Primary Biliary Cirrhosis and Primary Sclerosing Cholangitis: a Review Featuring a Women's Health Perspective. Journal of clinical and translational hepatology 2014;2:266-284.

13. Desmet VJ. Histopathology of chronic cholestasis and adult ductopenic syndrome. Clinics in liver disease 1998;2:249-viii.

14. Lee YM, Kaplan MM. Primary sclerosing cholangitis. The New England journal of medicine 1995;332:924-933.

15. Ludwig J, Dickson ER, McDonald GS. Staging of chronic nonsuppurative destructive cholangitis (syndrome of primary biliary cirrhosis). Virchows Archiv. A, Pathological anatomy and histology 1978;379:103-112.

16. Lazaridis KN, LaRusso NF. Primary Sclerosing Cholangitis. The New England journal of medicine 2016;375:1161-1170.

17. Karlsen TH, Folseraas T, Thorburn D, Vesterhus M. Primary sclerosing cholangitis - a comprehensive review. Journal of hepatology 2017;67:1298-1323.

18. Pinzani M, Luong TV. Pathogenesis of biliary fibrosis. Biochimica et biophysica acta. Molecular basis of disease 2018;1864:1279-1283.

19. Guicciardi ME, Trussoni CE, Krishnan A, Bronk SF, Lorenzo Pisarello MJ, O'Hara SP, Splinter PL, et al. Macrophages contribute to the pathogenesis of sclerosing cholangitis in mice. Journal of hepatology 2018;69:676-686.

20. Tacke F, Zimmermann HW. Macrophage heterogeneity in liver injury and fibrosis. Journal of hepatology 2014;60:1090-1096.

21. Koyama Y, Brenner DA. Liver inflammation and fibrosis. The Journal of clinical investigation 2017;127:55-64.

22. Schuppan D, Surabattula R, Wang XY. Determinants of fibrosis progression and regression in NASH. Journal of hepatology 2018;68:238-250.

23. Karlmark KR, Weiskirchen R, Zimmermann HW, Gassler N, Ginhoux F, Weber C, Merad M, et al. Hepatic recruitment of the inflammatory Gr1+ monocyte subset upon liver injury promotes hepatic fibrosis. Hepatology (Baltimore, Md.) 2009;50:261-274.

24. Wang M, You Q, Lor K, Chen F, Gao B, Ju C. Chronic alcohol ingestion modulates hepatic macrophage populations and functions in mice. Journal of leukocyte biology 2014;96:657-665.

25. Govaere O, Cockell S, Van Haele M, Wouters J, Van Delm W, Van den Eynde K, Bianchi A, et al. High-throughput sequencing identifies aetiology-dependent differences in ductular reaction in human chronic liver disease. The Journal of pathology 2019;248:66-76.

26. Sato K, Marzioni M, Meng F, Francis H, Glaser S, Alpini G. Ductular Reaction in Liver Diseases: Pathological Mechanisms and Translational Significances. Hepatology (Baltimore, Md.) 2019;69:420-430.

27. Roskams TA, Theise ND, Balabaud C, Bhagat G, Bhathal PS, Bioulac-Sage P, Brunt EM, et al. Nomenclature of the finer branches of the biliary tree: canals, ductules, and ductular reactions in human livers. Hepatology (Baltimore, Md.) 2004;39:1739-1745.

28. Crosby HA, Hubscher S, Fabris L, Joplin R, Sell S, Kelly D, Strain AJ. Immunolocalization of putative human liver progenitor cells in livers from patients with end-stage primary biliary cirrhosis and sclerosing cholangitis using the monoclonal antibody OV-6. The American journal of pathology 1998;152:771-779.

29. Hahn E, Wick G, Pencev D, Timpl R. Distribution of basement membrane proteins in normal and fibrotic human liver: collagen type IV, laminin, and fibronectin. Gut 1980;21:63-71.

30. Bataller R, Brenner DA. Liver fibrosis. The Journal of clinical investigation 2005;115:209-218.

31. Hernandez-Gea V, Friedman SL. Pathogenesis of liver fibrosis. Annual review of pathology 2011;6:425-456.

32. Higashi T, Friedman SL, Hoshida Y. Hepatic stellate cells as key target in liver fibrosis. Advanced drug delivery reviews 2017;121:27-42.

33. Zhang Z, Yao Z, Zhao S, Shao J, Chen A, Zhang F, Zheng S. Interaction between autophagy and senescence is required for dihydroartemisinin to alleviate liver fibrosis. Cell death & disease 2017;8:e2886-e2886.

34. Meng L, Quezada M, Levine P, Han Y, McDaniel K, Zhou T, Lin E, et al. Functional role of cellular senescence in biliary injury. The American journal of pathology 2015;185:602-609.

35. Rapisarda V, Borghesan M, Miguela V, Encheva V, Snijders AP, Lujambio A, O'Loghlen A. Integrin Beta 3 Regulates Cellular Senescence by Activating the TGF-β Pathway. Cell reports 2017;18:2480-2493.

36. Tabibian JH, Trussoni CE, O'Hara SP, Splinter PL, Heimbach JK, LaRusso NF. Characterization of cultured cholangiocytes isolated from livers of patients with primary sclerosing cholangitis. Laboratory investigation; a journal of technical methods and pathology 2014;94:1126-1133.

37. Tabibian JH, O'Hara SP, Splinter PL, Trussoni CE, LaRusso NF. Cholangiocyte senescence by way of N-ras activation is a characteristic of primary sclerosing cholangitis. Hepatology (Baltimore, Md.) 2014;59:2263-2275.

38. Oude Elferink RPJ, Paulusma CC. Function and pathophysiological importance of ABCB4 (MDR3 P-glycoprotein). Pflugers Archiv : European journal of physiology 2007;453:601-610.

39. Smit JJ, Schinkel AH, Oude Elferink RP, Groen AK, Wagenaar E, van Deemter L, Mol CA, et al. Homozygous disruption of the murine mdr2 P-glycoprotein gene leads to a complete absence of phospholipid from bile and to liver disease. Cell 1993;75:451-462.

40. Fickert P, Fuchsbichler A, Wagner M, Zollner G, Kaser A, Tilg H, Krause R, et al. Regurgitation of bile acids from leaky bile ducts causes sclerosing cholangitis in Mdr2 (Abcb4) knockout mice. Gastroenterology 2004;127:261-274.

41. Eaton JE, Talwalkar JA, Lazaridis KN, Gores GJ, Lindor KD. Pathogenesis of primary sclerosing cholangitis and advances in diagnosis and management. Gastroenterology 2013;145:521-536.

42. Popov Y, Patsenker E, Fickert P, Trauner M, Schuppan D. Mdr2 (Abcb4)-/- mice spontaneously develop severe biliary fibrosis via massive dysregulation of pro- and antifibrogenic genes. Journal of hepatology 2005;43:1045-1054.

43. Sato K, Glaser S, Kennedy L, Liangpunsakul S, Meng F, Francis H, Alpini G. Preclinical insights into cholangiopathies: disease modeling and emerging therapeutic targets. Expert opinion on therapeutic targets 2019;23:461-472.

44. Lamouille S, Xu J, Derynck R. Molecular mechanisms of epithelial-mesenchymal transition. Nature reviews. Molecular cell biology 2014;15:178-196.

45. Carpino G, Cardinale V, Renzi A, Hov JR, Berloco PB, Rossi M, Karlsen TH, et al. Activation of biliary tree stem cells within peribiliary glands in primary sclerosing cholangitis. Journal of hepatology 2015;63:1220-1228.

46. Nakagawa H, Hikiba Y, Hirata Y, Font-Burgada J, Sakamoto K, Hayakawa Y, Taniguchi K, et al. Loss of liver E-cadherin induces sclerosing cholangitis and promotes carcinogenesis. Proceedings of the National Academy of Sciences of the United States of America 2014;111:1090-1095.

47. Rygiel KA, Robertson H, Marshall HL, Pekalski M, Zhao L, Booth TA, Jones DEJ, et al. Epithelial-mesenchymal transition contributes to portal tract fibrogenesis during human chronic liver disease. Laboratory investigation; a journal of technical methods and pathology 2008;88:112-123.

48. Fabris L, Brivio S, Cadamuro M, Strazzabosco M. Revisiting Epithelial-to-Mesenchymal Transition in Liver Fibrosis: Clues for a Better Understanding of the "Reactive" Biliary Epithelial Phenotype. Stem cells international 2016;2016:2953727-2953727.

49. Taura K, Iwaisako K, Hatano E, Uemoto S. Controversies over the Epithelial-to-Mesenchymal Transition in Liver Fibrosis. Journal of clinical medicine 2016;5:9.

50. Chu AS, Diaz R, Hui J-J, Yanger K, Zong Y, Alpini G, Stanger BZ, et al. Lineage tracing demonstrates no evidence of cholangiocyte epithelial-to-mesenchymal transition in murine models of hepatic fibrosis. Hepatology (Baltimore, Md.) 2011;53:1685-1695.

51. Scholten D, Osterreicher CH, Scholten A, Iwaisako K, Gu G, Brenner DA, Kisseleva T. Genetic labeling does not detect epithelial-to-mesenchymal transition of cholangiocytes in liver fibrosis in mice. Gastroenterology 2010;139:987-998.

52. Lowery J, Kuczmarski ER, Herrmann H, Goldman RD. Intermediate Filaments Play a Pivotal Role in Regulating Cell Architecture and Function. The Journal of biological chemistry 2015;290:17145-17153.

53. Mendez MG, Kojima S-I, Goldman RD. Vimentin induces changes in cell shape, motility, and adhesion during the epithelial to mesenchymal transition. FASEB journal : official publication of the Federation of American Societies for Experimental Biology 2010;24:1838-1851.

54. Lehtinen L, Ketola K, Mäkelä R, Mpindi J-P, Viitala M, Kallioniemi O, Iljin K. High-throughput RNAi screening for novel modulators of vimentin expression identifies MTHFD2 as a regulator of breast cancer cell migration and invasion. Oncotarget 2013;4:48-63.

55. Satelli A, Li S. Vimentin in cancer and its potential as a molecular target for cancer therapy. Cellular and molecular life sciences : CMLS 2011;68:3033-3046.

56. Alpini G, Lenzi R, Sarkozi L, Tavoloni N. Biliary physiology in rats with bile ductular cell hyperplasia. Evidence for a secretory function of proliferated bile ductules. The Journal of clinical investigation 1988;81:569-578.

57. Glaser S, Lam IP, Franchitto A, Gaudio E, Onori P, Chow BK, Wise C, et al. Knockout of secretin receptor reduces large cholangiocyte hyperplasia in mice with

extrahepatic cholestasis induced by bile duct ligation. Hepatology (Baltimore, Md.) 2010;52:204-214.

58. Glaser S, Meng F, Han Y, Onori P, Chow BK, Francis H, Venter J, et al. Secretin stimulates biliary cell proliferation by regulating expression of microRNA 125b and microRNA let7a in mice. Gastroenterology 2014;146:1795-1808.e1712.

59. Alpini G, Glaser S, Robertson W, Rodgers RE, Phinizy JL, Lasater J, LeSage GD. Large but not small intrahepatic bile ducts are involved in secretin-regulated ductal bile secretion. The American journal of physiology 1997;272:G1064-G1074.

60. Alpini G, Ulrich CD, 2nd, Phillips JO, Pham LD, Miller LJ, LaRusso NF. Upregulation of secretin receptor gene expression in rat cholangiocytes after bile duct ligation. The American journal of physiology 1994;266:G922-G928.

61. Francis H, McDaniel K, Han Y, Liu X, Kennedy L, Yang F, McCarra J, et al. Regulation of the extrinsic apoptotic pathway by microRNA-21 in alcoholic liver injury. The Journal of biological chemistry 2014;289:27526-27539.

62. Han Y, Onori P, Meng F, DeMorrow S, Venter J, Francis H, Franchitto A, et al. Prolonged exposure of cholestatic rats to complete dark inhibits biliary hyperplasia and liver fibrosis. American journal of physiology. Gastrointestinal and liver physiology 2014;307:G894-G904.

63. Alpini G, Phillips JO, Vroman B, LaRusso NF. Recent advances in the isolation of liver cells. Hepatology (Baltimore, Md.) 1994;20:494-514.

64. Ishii M, Vroman B, LaRusso NF. Isolation and morphologic characterization of bile duct epithelial cells from normal rat liver. Gastroenterology 1989;97:1236-1247.

65. Glaser SS, Rodgers RE, Phinizy JL, Robertson WE, Lasater J, Caligiuri A, Tretjak Z, et al. Gastrin inhibits secretin-induced ductal secretion by interaction with specific receptors on rat cholangiocytes. The American journal of physiology 1997;273:G1061-G1070.

66. Meadows V, Kennedy L, Hargrove L, Demieville J, Meng F, Virani S, Reinhart E, et al. Downregulation of hepatic stem cell factor by Vivo-Morpholino treatment inhibits mast cell migration and decreases biliary damage/senescence and liver fibrosis in Mdr2(-/-) mice. Biochimica et biophysica acta. Molecular basis of disease 2019;1865:165557-165557.

67. Meng F, Onori P, Hargrove L, Han Y, Kennedy L, Graf A, Hodges K, et al. Regulation of the histamine/VEGF axis by miR-125b during cholestatic liver injury in mice. The American journal of pathology 2014;184:662-673.

68. Puche JE, Lee YA, Jiao J, Aloman C, Fiel MI, Muñoz U, Kraus T, et al. A novel murine model to deplete hepatic stellate cells uncovers their role in amplifying liver damage in mice. Hepatology (Baltimore, Md.) 2013;57:339-350.

69. Wan Y, Ceci L, Wu N, Zhou T, Chen L, Venter J, Francis H, et al. Knockout of α-calcitonin gene-related peptide attenuates cholestatic liver injury by differentially regulating cellular senescence of hepatic stellate cells and cholangiocytes. Laboratory investigation; a journal of technical methods and pathology 2019;99:764-776.

70. Wan Y, Meng F, Wu N, Zhou T, Venter J, Francis H, Kennedy L, et al. Substance P increases liver fibrosis by differential changes in senescence of cholangiocytes and hepatic stellate cells. Hepatology (Baltimore, Md.) 2017;66:528-541.

71. Zhang Y, Xu N, Xu J, Kong B, Copple B, Guo GL, Wang L. E2F1 is a novel fibrogenic gene that regulates cholestatic liver fibrosis through the Egr-1/SHP/EID1 network. Hepatology (Baltimore, Md.) 2014;60:919-930.

72. Liu J, Eischeid AN, Chen X-M. Col1A1 production and apoptotic resistance in TGF-β1-induced epithelial-to-mesenchymal transition-like phenotype of 603B cells. PloS one 2012;7:e51371-e51371.

73. Xia J-L, Dai C, Michalopoulos GK, Liu Y. Hepatocyte growth factor attenuates liver fibrosis induced by bile duct ligation. The American journal of pathology 2006;168:1500-1512.

74. Ren XF, Mu LP, Jiang YS, Wang L, Ma JF. LY2109761 inhibits metastasis and enhances chemosensitivity in osteosarcoma MG-63 cells. European review for medical and pharmacological sciences 2015;19:1182-1190.

75. Lv H, Liu L, Zhang Y, Song T, Lu J, Chen X. Ingenuity pathways analysis of urine metabonomics phenotypes toxicity of gentamicin in multiple organs. Molecular bioSystems 2010;6:2056-2067.

76. Wan Y, McDaniel K, Wu N, Ramos-Lorenzo S, Glaser T, Venter J, Francis H, et al. Regulation of Cellular Senescence by miR-34a in Alcoholic Liver Injury. The American journal of pathology 2017;187:2788-2798.

77. Choi SS, Syn W-K, Karaca GF, Omenetti A, Moylan CA, Witek RP, Agboola KM, et al. Leptin promotes the myofibroblastic phenotype in hepatic stellate cells by activating the hedgehog pathway. The Journal of biological chemistry 2010;285:36551-36560.

78. Sung R, Lee SH, Ji M, Han J-H, Kang MH, Kim JH, Choi J-W, et al. Epithelial-mesenchymal transition-related protein expression in biliary epithelial cells associated with hepatolithiasis. Journal of gastroenterology and hepatology 2014;29:395-402.

79. Kang Y, Massagué J. Epithelial-mesenchymal transitions: twist in development and metastasis. Cell 2004;118:277-279.

80. Sato Y, Harada K, Ozaki S, Furubo S, Kizawa K, Sanzen T, Yasoshima M, et al. Cholangiocytes with mesenchymal features contribute to progressive hepatic fibrosis of the polycystic kidney rat. The American journal of pathology 2007;171:1859-1871.

81. Dan YY, Riehle KJ, Lazaro C, Teoh N, Haque J, Campbell JS, Fausto N. Isolation of multipotent progenitor cells from human fetal liver capable of differentiating into liver and mesenchymal lineages. Proceedings of the National Academy of Sciences of the United States of America 2006;103:9912-9917.

82. Kennedy L, Hargrove L, Demieville J, Karstens W, Jones H, DeMorrow S, Meng F, et al. Blocking H1/H2 histamine receptors inhibits damage/fibrosis in Mdr2(-/-) mice and human cholangiocarcinoma tumorigenesis. Hepatology (Baltimore, Md.) 2018;68:1042-1056.

83. Fabris L, Strazzabosco M. Epithelial-mesenchymal interactions in biliary diseases. Seminars in liver disease 2011;31:11-32.

84. Fickert P, Pollheimer MJ, Beuers U, Lackner C, Hirschfield G, Housset C, Keitel V, et al. Characterization of animal models for primary sclerosing cholangitis (PSC). Journal of hepatology 2014;60:1290-1303.

85. Morita S-y, Terada T. Molecular mechanisms for biliary phospholipid and drug efflux mediated by ABCB4 and bile salts. BioMed research international 2014;2014:954781-954781.

86. Yanguas SC, Cogliati B, Willebrords J, Maes M, Colle I, van den Bossche B, de Oliveira CPMS, et al. Experimental models of liver fibrosis. Archives of toxicology 2016;90:1025-1048.

87. Kim E, Lisby A, Ma C, Lo N, Ehmer U, Hayer KE, Furth EE, et al. Promotion of growth factor signaling as a critical function of β-catenin during HCC progression. Nature communications 2019;10:1909-1909.

88. Rodriguez FJ, Lewis-Tuffin LJ, Anastasiadis PZ. E-cadherin's dark side: possible role in tumor progression. Biochimica et biophysica acta 2012;1826:23-31.

89. Wei Y, Van Nhieu JT, Prigent S, Srivatanakul P, Tiollais P, Buendia M-A. Altered expression of E-cadherin in hepatocellular carcinoma: correlations with genetic alterations, beta-catenin expression, and clinical features. Hepatology (Baltimore, Md.) 2002;36:692-701.

90. Gonzalez DM, Medici D. Signaling mechanisms of the epithelial-mesenchymal transition. Science signaling 2014;7:re8-re8.

91. Patsenker E, Popov Y, Stickel F, Jonczyk A, Goodman SL, Schuppan D. Inhibition of integrin alphavbeta6 on cholangiocytes blocks transforming growth factor-beta activation and retards biliary fibrosis progression. Gastroenterology 2008;135:660-670.

92. Harada K, Sato Y, Ikeda H, Isse K, Ozaki S, Enomae M, Ohama K, et al. Epithelial-mesenchymal transition induced by biliary innate immunity contributes to the sclerosing cholangiopathy of biliary atresia. The Journal of pathology 2009;217:654-664.

93. Nakanuma Y, Sasaki M, Harada K. Autophagy and senescence in fibrosing cholangiopathies. Journal of hepatology 2015;62:934-945.

94. Alvaro D, Mancino MG, Glaser S, Gaudio E, Marzioni M, Francis H, Alpini G. Proliferating cholangiocytes: a neuroendocrine compartment in the diseased liver. Gastroenterology 2007;132:415-431.

95. Maroni L, Haibo B, Ray D, Zhou T, Wan Y, Meng F, Marzioni M, et al. Functional and structural features of cholangiocytes in health and disease. Cellular and molecular gastroenterology and hepatology 2015;1:368-380.

96. Guerrier M, Attili F, Alpini G, Glaser S. Prolonged administration of secretin to normal rats increases biliary proliferation and secretin-induced ductal secretory activity. Hepatobiliary surgery and nutrition 2014;3:118-125.

97. Loarca L, De Assuncao TM, Jalan-Sakrikar N, Bronk S, Krishnan A, Huang B, Morton L, et al. Development and characterization of cholangioids from normal and diseased human cholangiocytes as an in vitro model to study primary sclerosing cholangitis. Laboratory investigation; a journal of technical methods and pathology 2017;97:1385-1396.

98. Shimizu R, Kanno K, Sugiyama A, Ohata H, Araki A, Kishikawa N, Kimura Y, et al. Cholangiocyte senescence caused by lysophosphatidylcholine as a potential

implication in carcinogenesis. Journal of hepato-biliary-pancreatic sciences 2015;22:675-682.

99. Han Y, Glaser S, Meng F, Francis H, Marzioni M, McDaniel K, Alvaro D, et al. Recent advances in the morphological and functional heterogeneity of the biliary epithelium. Experimental biology and medicine (Maywood, N.J.) 2013;238:549-565.